Heliyon 10 (2024) e28648

Contents lists available at ScienceDirect

Heliyon

journal homepage: www.cell.com/heliyon

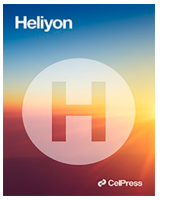

Research article

A graphene oxide based composite granule for methylene blue separation from aqueous solution: Adsorption, kinetics and thermodynamic studies

Huynh Vu Thanh Luong [a,b,*], Thanh Phu Le [a,b], Tran Lan Trinh Le [a,b], Huynh Giao Dang [a,b], Thi Bich Quyen Tran [a]

[a] Faculty of Chemical Engineering, Can Tho University, 3/2 Street, Ninh Kieu District, Can Tho 94000, Viet Nam
[b] Applied Chemical Engineering Labotarary, Can Tho University, 3/2 Street, Ninh Kieu District, Can Tho 94000, Viet Nam

ARTICLE INFO

Keywords:
Graphene oxide-chitosan
Granular adsorbent
Methylene blue
Recyclic stability

ABSTRACT

Graphene oxide and chitosan composite material using as a high-efficiency and low-cost granular adsorbent for methylene blue removal was fabricated via self-assembling method. The effects of pH value, contact time, initial concentration, adsorbent dose, temperature, and recyclic stability on the adsorption performance of methylene blue in aqueous solution were investigated in detail. Desorption process with the effects of solvents, contact time, and temperature were also conducted carefully in this study. The adsorption kinetics and adsorption isotherm of dye adsorption process showed that dye adsorption process was fitted to the pseudo-second-order kinetic model and the Freundlich adsorption isotherm, indicating a physical adsorption process with multilayer adsorption. The intra-particle diffusion model indicated that the dye adsorption by the granular adsorbent was strongly happened during the first 4 h. The thermodynamic study showed that the adsorption was a spontaneous and exothermic process and dye ions were condensed onto the surface of adsorbent. The maximum adsorption capacity of dye on the granular adsorbent was calculated as 951.35 mg/g and the adsorbent could maintain its adsorption performance after six cycles. In general, this study provided an efficient, cost-effective, and recyclable the granular adsorbent for dye separation from aqueous solution.

1. Introduction

In modern society, increase in industrialization and population has occurred fast and resulted in water pollution in many developing countries and regions. One of the main challenges in wastewater treatments recently is persistent organic compounds [1]. Dye, one kind of persistent organic compounds, is widely utilized in numerous industrial sectors, i.e. food, textile, cosmetics, printing, and paper [2]. As a result, organic dye pollution has become one of the most serious risks to human health like immune response, carcinogen, or chronic effects [3,4], attributing to increasing of organic dyes quantity in the environment, as well as to their aromatic structures making them stable in the presence of light, heat, or oxidants [1,2]. Consequently, it is critical to find an efficient method to separate and eliminate the dyes found in wastewater before discharging them into the environment.

* Corresponding author. Faculty of Chemical Engineering, Can Tho University, Campus II, 3/2 Street, Ninh Kieu District, Can Tho 94000, Viet Nam.
E-mail address: lhvthanh@ctu.edu.vn (H.V.T. Luong).

https://doi.org/10.1016/j.heliyon.2024.e28648
Received 4 February 2024; Received in revised form 20 March 2024; Accepted 21 March 2024
Available online 22 March 2024

Many methods, including coagulation-flocculation, adsorption, ion exchange, oxidation and advanced oxidation, electrochemical and photochemical degradation, have been used in recent years to separate dyes in wastewater, becoming the primary research direction of wastewater purification [5–7]. Among these treatment procedures, adsorption has stood out as an appealing way for treating water pollution, especially in many developing nations, because of easy operation, low cost, and high efficiency [8]. In the adsorption method, adsorbents play an essential role for removing contaminants. Many adsorption materials have been researched, such as carbon nanotubes, zeolite, activated carbon, and graphene-based composite materials due to their high surface area, porosity percentage and/or cation exchange capacity [9,10]. Standing out of these materials, graphene has emerged as a material of interest in these investigations because of its unique mechanical, thermal, and electrical characteristics. However, its application is limited because of its poor solubility, easy agglomeration, and difficult synthesis [11]. As an alternative, graphene oxide (GO) is one of several graphene derivatives created by chemically exfoliating raw graphite. GO has a large specific surface area and a high dispersion of oxygen-containing groups [11–13]. Nevertheless, it is difficult to recycle GO after adsorption due to its high dispersibility [12]. The drawback of GO recovery may be efficiently addressed by combining GO and polymers into a gel [13]. The polymers commonly used to combine with GO to form a gel for wastewater treatment are polyamides [14], epoxy [15], tannic acid [16], and chitosan [17]. Compared to other polymers, chitosan (CS), a high-performance and environmentally acceptable natural polymeric substance with several sources, has a large number of free amino groups being positively charged throughout a wide pH range. Integrating GO with CS obtains a versatile adsorbent because of their advantages [18]. To improve its adsorption capacity and enhance the removal efficiency, the design and functionalization of novel adsorbent still need to be explored [19]. Chitosan has one amino group and two hydroxyl groups on each glucosamine monomer that act as adsorption sites, especially the amino groups which are strongly interactive with metal ions. Moreover, the applications of chitosan are limited because of its solubility in acid solutions. Hence, it is necessary to crosslink chitosan in order to make it stable in acid solutions. The functionalization of chitosan can be done among diverse types of a polar functional group, i.e. graphene oxide, and numerous graphene-based composite materials have synthesized for the removal of various environmental contaminants, which combined GO and chitosan through coordination, electrostatic interaction, and covalent interaction which produces chitosan/GO composites [20,21]. Studies have been conducted on combining the properties of graphene oxide with chitosan in order to construct hydrogel adsorbent materials [22,23] and GO/Chitosan membranes for adsorption applications [16,24]. These materials combining GO and Chitosan have demonstrated exceptional adsorption characteristics, but they need a highly intricate fabrication process, particularly for industrial wastewater treatment using adsorption systems granular adsorbent material would be the most appropriate choice [25,26].

In our understanding, there is no work published on the process for fabricating GO/CS granular adsorbents, as well as the use of GO/CS granular adsorbents to remove methylene blue and deeply study the adsorption, kinetic and thermodynamics of using this material for methylene blue removal.

Furthermore, the economic benefits of recycling adsorbent materials have not been investigated and analyzed yet. In this work, a GO/CS granular adsorbent has been prepared by self-assembly method, being cross-linked in glutaraldehyde by mutual reaction between amino groups on CS and oxygen-containing acidic ones on GO. The methylene blue (MB) adsorption capacity of the GO/CS adsorbent are assessed via affecting parameters, such as pH, contact time, initial concentration, adsorbent dose, and temperature. The kinetic, thermodynamic and adsorption isotherms of methylene blue adsorption using GO/CS are also evaluated in this study. To assess potential of industrial application, the adsorbent recycling is conducted by adsorption-desorption evaluation.

2. Materials and methods

2.1. Materials

In this study, expandable graphite (99.8%, 300 meshes) was provided by Qingdao Henglid graphite company in China. Chitosan (Degree of deacetylation >80%, viscosity average molar mass of 87 kDa) was collected from S-Green company in Vietnam. Xilong supplied methylene blue (MB, $C_{16}H_{18}N_3ClS{\cdot}3H_2O$, 99%), acetic acid ($CH_3COOH$, >99.5), hydrochloric acid (HCl, 36–38%), sodium hydroxide (NaOH, >98%) and glutaraldehyde (37%). Stock solutions of dyes were prepared in deionized (DI) water and further diluted to the required working concentrations.

2.2. Synthesis of graphene oxide (GO)

In this work, GO was prepared by using the Hummers' method [27]. In detail, the beaker containing 230 mL of concentrated H_2SO_4 was first added with 5 g of expanded graphite and 5 g of $NaNO_3$, then thoroughly distributed with a magnetic stirrer (MISUNG, HS180). Subsequently, 5 g of $KMnO_4$ was gently added and fully disseminated in the mixture. The mixture produced by the preceding process was then carried out and stored in an ice bath at 273 K, atmosphere for 24 h. After that, the mixture was removed out of the ice bath and heated to 308 K in an oil bath for 30 min while stirring continuously until the mixture turned brownish. While heating, the temperature of the mixture gradually rose to 371 K and 460 mL of DI water was added to the mixture. The mixture was subsequently agitated to form a suspension via stirring for 15 min at 371 K. After cooling down to ambient temperature, the suspension was treated with 3% hydrogen peroxide until becoming brilliant yellow. The metal ions in the solution were removed by washing with 15 mL of HCl 5%. Next, the suspension was rinsed many times with DI water until neutral. Finally, GO was obtained via drying the solid in vacuum drier (Memmert VO101) at pressure of 0.6 bar and temperature of 60 °C for 4 h.

2.3. Synthesis of graphene oxide/chitosan (GO/CS) granules

The GO/CS granules in this study were produced by self-assembly method. To this end, chitosan (DDA >80%) was first dissolved in 1% acetic acid solution for 12 h to prepare CS solutions of 1.5%, 3%, 5%, and 10%. In the meantime, 0.15 g GO was dispersed in DI water at room temperature via ultrasonic device (Vevey, KQ-300DA) with a power of 300 W for 30 min to obtain a 1.5% GO suspension mixture (w/v). This GO suspension mixture and CS solutions were magnetically stirred at the speed of 450 rpm for 30 min at room temperature. The mixture was then placed into a 10-mL syringe and dropped down to a NaOH solution with concentration ranging from 0.5 to 2 M. The GO/CS granules were subsequently immersed in NaOH solution for 2 h. The GO/CS granules were then removed out of NaOH solution and washed with DI water until to pH 7.0 before immersing again in a 25% glutaraldehyde solution for 2 h, 3 h, 8 h, and 12 h, respectively. These granules after that were separated out of the glutaraldehyde solution and dried at pressure of 0.6 bar and temperature of 60 °C for 4 h, and then sieved with standard sieve No. 16 and No. 18 (AS2000 Control, Retsh) to obtain the GO/CS granular adsorbent in size of 1.0–1.12 mm.

2.4. Characterization of the GO/chitosan

The surface microstructure of the as-synthesized GO/CS granules was characterized via a scanning electron microscopy (S-4800 High-resolution SEM, Hitachi). To evaluate the changes of functional groups on the surface of GO, CS, and both fresh and used GO/CS granular absorbent, Fourier transform infrared (FT-IR) spectroscopy was employed. The FT-IR spectra are obtained using a NICOLET 6700 (Thermo) spectrophotometer (frequency range from 4000 to 500 cm^{-1}) with KBr pellet method. All analyses were conducted under a dry air purge at co-addition of 256 interferograms collected at 4.0 cm^{-1} resolution. The specific surface areas and pore size distribution curves of the materials were calculated using the Brunauer-Emmett-Teller (BET) method in a relative pressure range of 0.05–1.0 and the density functional theory method, respectively (Nova 1000e, Quantachrome). The gas adsorption method is a common method to measure the specific surface area and pore size distribution of materials.

2.5. MB adsorption experiments

The dye adsorption capacity was examined by placing the adsorbent in aqueous dye solutions, shaking (Digisystem laboratory, OS350D) at speed of 150 rpm. Before the adsorption process, the adsorbent was washed with DI water until pH around 7.0. The MB solution was prepared with a concentration of 100 (mg/L) before the adsorption test and diluted to desired concentrations required for the experiments. The effects of different parameters such as pH (2.0–10.0), initial MB concentration (5.0–30.0 mg/L), contact time (1–24 h), adsorbent dose (0.1–0.5 g) and temperature (30–50 °C) were conducted via alternating variable method. The concentration of MB at the beginning and equilibrium state was measured at maximum wavelength (λ_{max}) of 665 nm using UV–vis Spectrophotometer (Labomed, UVD-3500) using the standard curve method. The standard curve for analyzing MB concentration and maximum absorption wavelength is shown in Fig. 1. The adsorption efficiency and capacity of GO/CS granules were calculated by the following equations:

$$\text{Adsorption capacity } (q_{ad})\ (mg/g) = \frac{(C_0 - C_e).V}{M} \quad (1)$$

$$\text{Adsorption efficiency } (\%) = \frac{(C_0 - C_e)}{C_0} \text{ x } 100 \quad (2)$$

where V is volume of MB solution (L), M is mass of adsorbent used (mg), C_e is final concentration of MB (mg/L), C_0 is initial concentration of MB (mg/L).

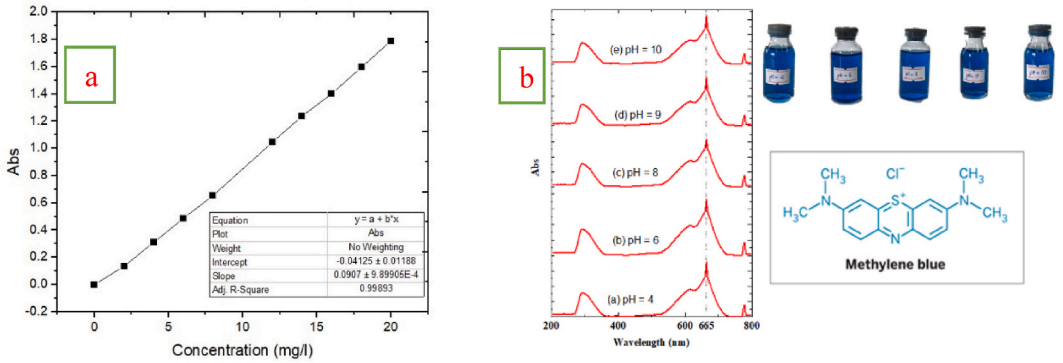

Fig. 1. The standard curve equation (a) and the maximum wavelength of MB at different pH levels (b).

2.6. Determination of pH_{pzc}

The point of zero charge, pH_{pzc}, of GO/CS adsorbent was determined using the method described by Nasiruddin Khan et al. [28]. Potassium chloride in concentrations of 0.1 M was used as a background electrolyte. The initial pH values (pH_i) of each solution were adjusted in range of 2 and 12 by small additions of 0.1 M of HCl or 0.1 M of NaOH and measured on pH meter (Ohaus, ST3100-F). In each initial solution 20 mL, 0.1000 g of GO/CS adsorbent was added into the beaker shaken at 150 rpm for 24 h at room temperature, centrifuged at 10,000 rpm for 10 min, and the pH of each supernatant was measured (pH_f). The pH_{pzc} of the samples was determined as the plateau of the curve $pH_f = f(pH_i)$.

2.7. MB desorption experiments

Desorption study of GO/CS adsorbent was performed by using combined effects of thermal, ultrasound and chemical regeneration. The spent adsorbent was heated to the temperature ranging from 40 to 80 °C with different solvents under effect of contact time from 1 to 6 h. In desorption experiments, the solvents including ethanol 70% (C_2H_5OH), sodium chloride 1 M (NaCl) and DI water (H_2O) were employed. Desorption capacity and efficiency of GO/CS adsorbent was calculated using equations (3) and (4).

$$\text{Desorption capacity } (q_{de})\ (\text{mg}/\text{g}) = \frac{(C_f).V}{M} \tag{3}$$

$$\text{Desorption efficiency } (\%) = \frac{(C_f)}{C_0} \text{ x } 100 \tag{4}$$

where V is volume of dye solution (L), M is mass of adsorbent used (mg), C_f is concentration of MB in solvent (mg/L), C_o is initial concentration of MB (mg/L).

The standard curve equation used to determine the MB concentration in this study was shown in Fig. 1a and b showed the maximum absorption wavelength of MB for different pH levels ranging from 4 to 10.

2.8. Adsorption kinetics models

2.8.1. Pseudo-first order model

MB molecules filled sites have a linear relationship with rate of adsorption/desorption. This assumption is made in pseudo-first order (PFO) reaction kinetics. The adsorption capacity of first-order rate expression can be expressed by equation (5). The intercept and slope of linear plot $\log(q_e\text{-}q_t)$ of versus t give the values of the adsorption rate constant (k_1) and equilibrium adsorption capacity (q_e), respectively [29].

$$\log(q_e - q_t) = \log q_e - \frac{K_1}{2.303} t \tag{5}$$

where k_1 (1/min) is the adsorption rate constant, k_1 and q_e are determined by plotting a fitted linear graph of $\log(q_e\text{-}q_t)$.

2.8.2. Pseudo-second order model

The pseudo-second-order (PSO) expresses that the square of the number of sites filled by dye molecules have linear relationship with rate of adsorption/desorption and can be express as follows [29,30]:

$$\frac{t}{q_t} = \frac{1}{k_2.q_e^2} + \frac{t}{q_e} \tag{6}$$

where k_2 (g/mg.min) represents a pseudo-second-order rate constant. Both k_2 and q_e can be obtained by plotting a fitted straight line graph with t as the X axis and t/q_t as the Y axis.

2.8.3. The intra-particle diffusion model

A study on the diffusion mechanism of GO/CS adsorbing MB is conducted by an intra-particle diffusion model. The mathematical expression of the intra-granular diffusion model is as follows [31].

$$q_{ref} = k_p\, t_{ref}^{1/2} + C \tag{7}$$

$$\left(\frac{q_t}{q_{ref}}\right) = 1 - R_i\left[1 - \left(\frac{t}{t_{ref}}\right)^{1/2}\right] \tag{8}$$

In the above formula, the intra-granular diffusion constant is k_p ($mg/g.min^{1/2}$). It can be obtained from the fitted line graph with $t^{1/2}$ as the X axis and q_t as the Y axis. R_i value is divided into five zones: Firstly, as $R_i = 1$ and $C/q_{ref} = 0$, there is no initial adsorption (zone 0). Next, when $1 > R_i > 0.9$ and $0 < C/q_{ref} < 0.1$, a weakly initial adsorption is occurring (zone 1). Then, if $0.9 > R_i > 0.5$ and $0.1 < C/q_{ref} < 0.5$, this is intermediately initial adsorption (zone 2). Subsequently, as $0.5 > R_i > 0.1$ and $0.5 < C/q_{ref} < 0.9$, a strongly initial

adsorption is observed (zone 3). Finally, when $R_i < 0.1$ and $C/q_{ref} > 0.9$, the initial adsorption is completely approaching (zone 4) [31].

2.9. Adsorption isotherms

2.9.1. Langmuir and Freundlich isotherm model

The interaction between GO/CS adsorbent and MB can be described by adsorption isotherms, in which Langmuir and Freundlich isotherm models are normally used to study equilibrium data. The Langmuir model proposes a monolayer adsorbate on the surface of the adsorbent, and it is based on the assumption that adsorption occurs on the homogeneous surface without interactions between the adsorbed dyes molecules, and no chemical reaction will occur. The Langmuir expression is as follows:

$$q_e = q_{max} \frac{k_L - C_e}{1 + k_L - C_e} \tag{9}$$

$$\frac{C_e}{q_e} = \frac{1}{q_{max} K_L} + \frac{C_e}{q_{max}} \tag{10}$$

where q_e (mg/g) is the amount of adsorbate adsorbed per mass of adsorbent; C_e (mg/L) is the equilibrium concentration of the adsorbate; q_{max} (mg/g) and K_L (L/mg) are Langmuir characteristic constants indicating maximum adsorption capacity and the energy of adsorption, respectively [32].

The Freundlich model assumes that adsorption occurs in the heterogeneous surface and it is expressed by equation (10).

$$q_e = k_F . C_e^{1/n} \tag{11}$$

$$\mathrm{Log} q_e = \frac{1}{n} . \log C_e + \log k_F \tag{12}$$

where q_e (mg/g) is the amount of adsorbate adsorbed per mass of adsorbent; C_e (mg/L) is the adsorbate equilibrium concentration; K_F (mg/g) and 1/n are Freundlich characteristic constants representing adsorption capacity and adsorption intensity, respectively [33].

2.9.2. Dubinin – radushkevich isotherm model

The Dubinin – Radushkevich (D–R) model is generally used to differentiate between physical and chemical adsorption and its linear form is given as:

$$\ln q_e = \ln q_m - \beta . \varepsilon^2 \tag{13}$$

where q_e is the amount of the dye adsorbed per mass of the adsorbent in (mg/g), β is a constant related to the mean free energy of adsorption per mole of the adsorbate (mol^2/J^2), ε is the Polanyi potential calculated from equation (14):

$$\varepsilon = RT \ln\left(1 + \frac{1}{C_e}\right) \tag{14}$$

The values of q_m and β can be computed from the slope and intercept of the plot of ln q_e. The constant β gives valuable information about the mean free energy E (kJ/mol) of adsorption per mole of adsorbate and it can be calculated using the following relationship:

$$E = \frac{1}{\sqrt{-2\beta}} \tag{15}$$

The value of E is valuable for appraising the type of adsorption process. When $E < 8.0$ kJ/mol, the adsorption can be described by physical interaction. Otherwise, the adsorption is chemical one [34].

2.9.3. The redlich-peterson isotherm model

The Redlich–Peterson equation is widely used as a compromise between Langmuir and Freundlich systems [35]. This model has three parameters and incorporates the advantageous significance of both models. Redlich–Peterson model can be represented as follows:

$$qe = \frac{ACe}{\left[1 + B(Ce)^{\beta}\right]} \tag{16}$$

where A (L/g) and B (L/mg) are the Redlich–Peterson isotherm constants and β is the exponent reflecting the heterogeneity of the sorbent, which lies between 0 and 1 [35].

2.10. Thermodynamic study

The parameters such as Gibbs free energy (ΔG^0), enthalpy (ΔH^0), and entropy (ΔS^0) are obtained through the Van't Hoff equation.

The expression is as follows [36,37].

$$\Delta G^0 = \Delta H^0 - T\Delta S^0 \tag{17}$$

$$\ln K_C = -\frac{\Delta H^0}{RT} + \frac{\Delta S^0}{R}$$

The constant of equilibrium (K_C) that is usually employed is given below:

$$K_C = \frac{C_o - C_e}{C_e} \tag{18}$$

where, T (K) and R (8.314 J/mol.K) are the absolute temperature and universal gas constant, respectively. K_C is the constant of equilibrium. The above mentioned parameters are obtained by drawing a fitted linear line graph of ln K_C relative to 1/T. C_e is final concentration of MB (mg/L), C_0 is initial concentration of MB (mg/L).

2.11. Statistical analysis

The experiments were triplicated and the results were presented in form of mean ± standard deviations (SD). In equilibrium isotherm modeling, no single isotherm can usually fit all the experimental data. The model predicted adsorption capacity, q_{ecal}, therefore, is compared with the experimental adsorption capacity, q_e, for each isotherm model in terms of the Sum of the Squares of the Errors calculated according to Eq. (18). It is indicator for accuracy, in which the best fit of the data can be assessed from the sum-of-squares value. The smallest value for SSE indicates the best fit data for the model [38].

$$SSE = \sum_{i=1}^{n} \left(q_{e,cal} - q_{e,exp}\right)^2 \tag{19}$$

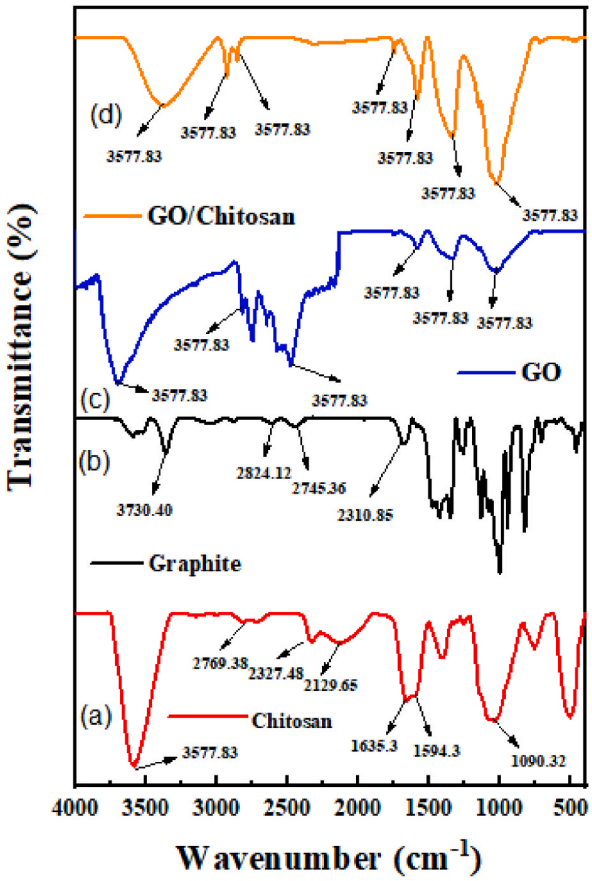

Fig. 2. FT-IR spectra of (a) Chitosan, (b) Graphite, (c) GO and (d) GO/Chitosan.

3. Results and discussion

3.1. Characterizations of the GO/CS granular adsorbent

3.1.1. FTIR analysis

Fourier Transform-infrared (FT-IR) spectroscopy is a diagnostic method for characterization of chitosan, graphene oxide and GO/CS cross-linked glutaraldehyde, and the results are shown in Fig. 2. The IR spectrum of the GO/Chitosan cross-linked glutaraldehyde (Fig. 2d) shows more different characteristic peaks than that of the pure chitosan (Fig. 2a) and the IR spectrum of the GO show in Fig. 2c. The results of the characterization of FT-IR on graphite sample shown in Fig. 2b completely agree with previous studies [39,40]. It was detected that graphite sample had a C]C bond. Absorption peak in Fig. 1b was found at wavenumber 1514.19 cm^{-1} showing the C]C bond as a characteristic of the graphite vibration band. Some functional group absorption bands were detected at wavenumber 3730.40 cm^{-1}, 2875.02 cm^{-1}, 2310.82 cm^{-1} indicating the absorption of the O–H, a methylene group in the C–H, and an acetylene group in the C ˆ C, respectively. There were a C–O vibration and a C–H bending vibration at wavenumber 1144.80 cm^{-1} and wavenumber 1291.40 cm^{-1}, respectively. The spectrum of GO (Fig. 2c) shows peaks at 1023.36, 1333.3, 1601.23, 2482.36 and 3452.41 cm^{-1} related to different oxygen containing functional groups corresponding to the C–O–C stretching vibrations, C–OH stretching, C–C stretching mode of sp^2 carbon skeleton, C–O stretching vibrations of the –COOH groups and –OH stretching vibration bonds, respectively. The FT-IR spectrum of GO completely agrees with previous studies [20,37,41]. Fig. 2a presents a peak at 3577.83 cm^{-1} corresponding to N–H stretching vibration of amino group, a peak at 1635.3 cm^{-1} corresponding to N–H bending vibration of $–NH_2$ and a peak at 1594 cm^{-1} corresponding to the C]O stretching vibration of amide [42,43]. The FT-IR spectrum of the GO/CS adsorbent shows a combination of characteristic peaks of CS and GO. Indeed, Fig. 2d presents the shift from peak at 1635.3 cm^{-1} of chitosan to peak at 1577.65 cm^{-1} of GO/CS designating the occurrence of amino-epoxy reaction [44]. A significant peak can be found at 1735.63 cm^{-1} corresponding to the formation of imine bond (C]N), i.e. Schiff's base structure by the reaction of amino groups of chitosan and aldehyde groups of glutaraldehyde. The formation of graphene oxide-chitosan composite may be due to the formation of covalent bonds after cross-linking between GO/CS with glutaraldehyde [44]. Finally, the GO/CS granules are successfully synthesized using self-assembly with glutaraldehyde as a cross-linker.

3.1.2. The UV–vis absorption of graphene oxide

The degree of oxidation can be determined by λ_{max} of UV–vis spectrum [45]. It can be seen from Fig. 3 that the absorption peak centered at around λ_{max} = 226 nm resembles $\pi \rightarrow \pi^*$ transition for C]C double bond of graphene oxide layers [46,47]. A shoulder observed at around 300 nm is attributed to $n \rightarrow \pi^*$ transition because of the C–O and C]O bonds on the graphene sheets [48]. The UV–Vis spectrum shows the higher value of λ_{max} for $\pi \rightarrow \pi^*$ electronic transition compared to $n \rightarrow \pi^*$ because the $\pi \rightarrow \pi^*$ transitions require less amount of energy due to the conjugation of C]C bonds of the graphene layers [49]. The results of this study are also consistent with recent reports on GO synthesis from coal by Sahoo et al. (2022) [50] showing that the synthesized GO had a maximum absorption wavelength at 226 nm, which characterized for the appearance of resembles $\pi \rightarrow \pi^*$ transition for C]C double bond of GO. From the UV–vis results, it can confirm that GO in this study was successfully synthesized using the Hummers' method.

3.1.3. FE-SEM analysis

The surface morphology of pure GO and GO/CS granules are determined via digital and FE-SEM images (Fig. 4). Fig. 4a shows the

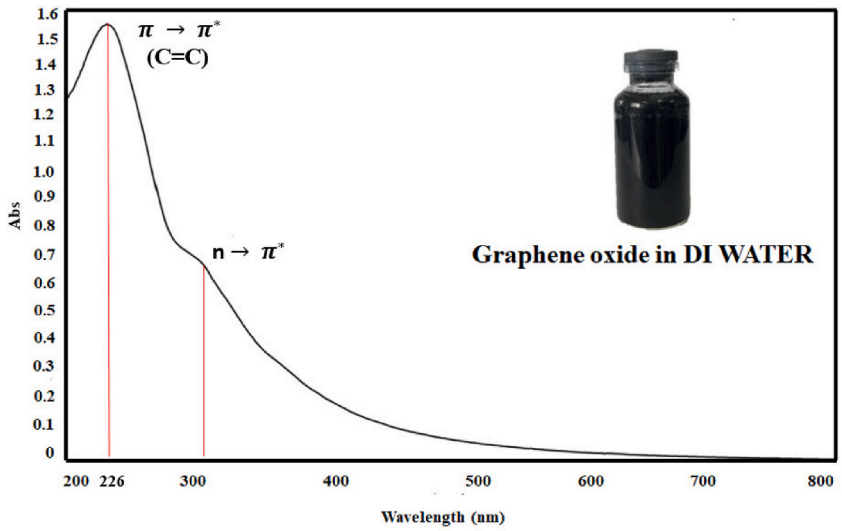

Fig. 3. The UV–vis absorption of graphene oxide.

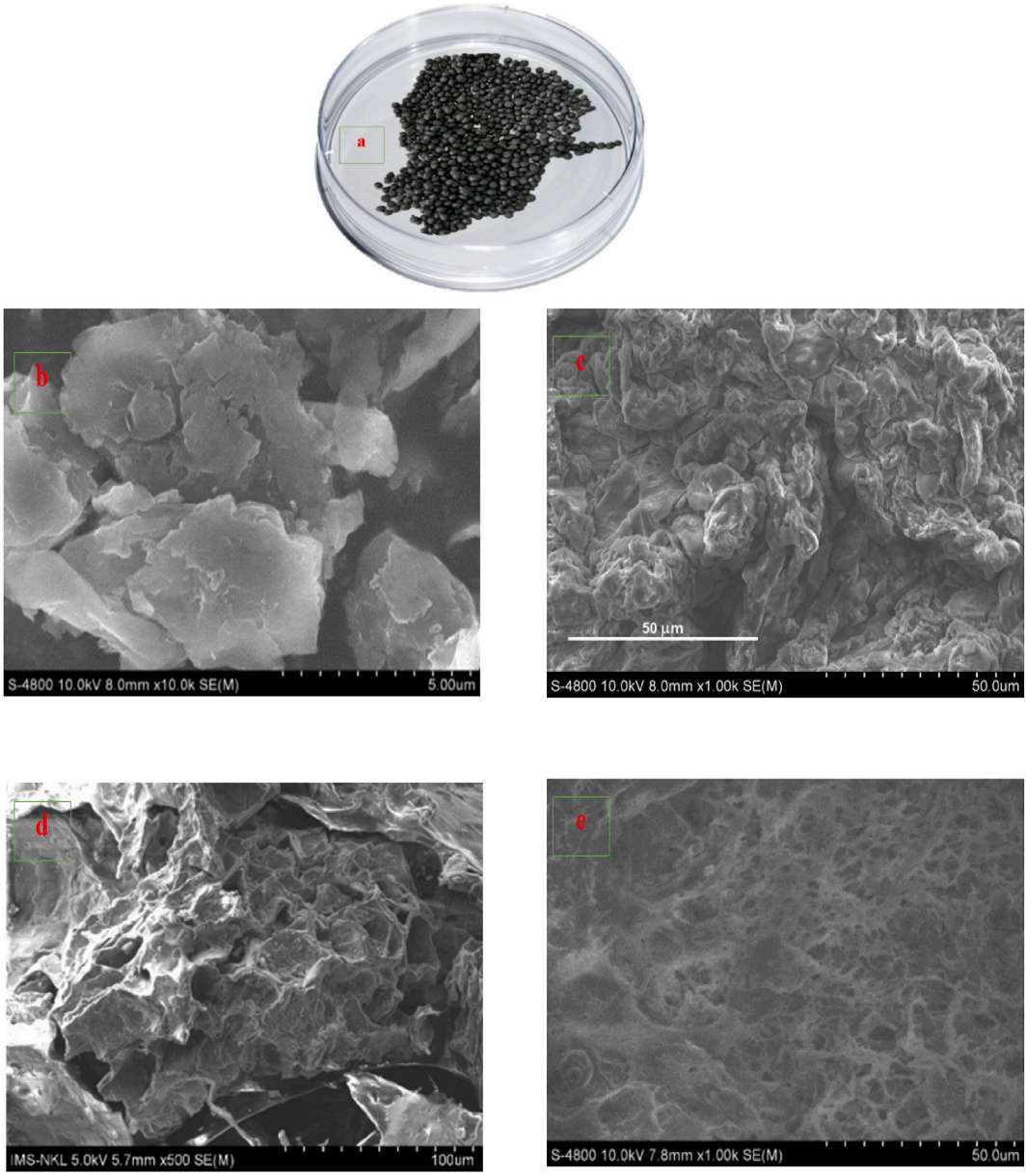

Fig. 4. Digital image of GO/CS granules (a) and FE-SEM images of pure GO (b) (c) and GO/CS granules (d), (e) at different magnification.

GO/CS granules and its size calculated via integrated sieving method is 1.05 ± 0.04 mm. The FE-SEM images of pure GO in Fig. 4b and c depict further revealing the layered structure of synthesized GO. Materials have wrinkled edges with irregular shapes of dense interconnected layers [51]. In the meantime, Fig. 4d and e show the surface morphology of GO/CS granules and indicate that the adsorbents possess higher surface roughness compared to pure GO. Inside the adsorbent, many macro-pores are observed and these pores generate a dense network occurring upon formation of a cross-linked between GO and chitosan [52]. Therefore, these variations in morphology and textural properties provide a microporous structure for GO/CS granules, causing a longer time for the adsorbates to enter the adsorbent.

3.1.4. Nitrogen adsorption and desorption isotherms

The BET surface area of GO and GO/Chitosan in Fig. 5 and Table 1 was measured from the adsorption/desorption isotherm of N_2 at 77 K. The specific surface area of the GO shown in Table 1 is 99.055 m^2/g lower than 253.87 m^2/g of GO from the study reported by Nagi M. El-Shafai et al. (2020) [53], attributing to the application of the modified method and graphite source. The specific surface area of the GO/CS in Table 1 shows a value of 1.235 m^2/g which sharply decreases compared to pure GO. The decrease in surface area of GO/CS adsorbent can be attributed to the formation of the bonding between GO and chitosan via the formation of the cross-linking.

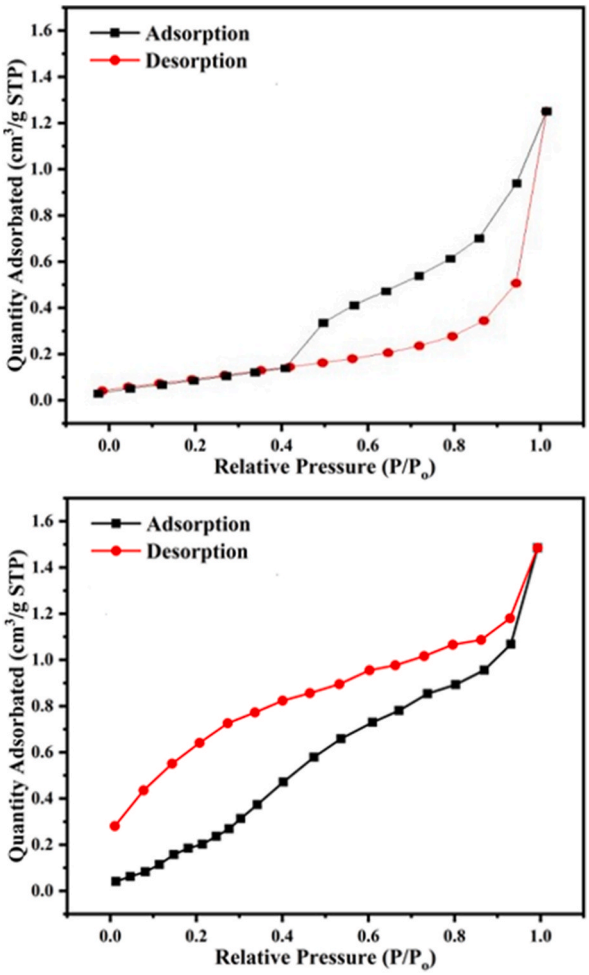

Fig. 5. Nitrogen adsorption/desorption isotherm of GO (a) and GO/CS (b) at 77 K.

Table 1
BET analysis results of GO and GO/CS materials.

Sample	S_{BET} [m^2/g]	Pore diameter [Å]	Pore volume [cm^3/g]	%micropore	%mesopore
GO	99.055	36.125	0.081	11.32	88.68
GO/CS	1.235	35.201	0.076	2.12	97.88

However, porous materials are mostly characterized in terms of pore diameters derived from gas adsorption-desorption data. The IUPAC conventions have proposed porous materials into six types of physisorption isotherms that reflect the relationship between sorption and porosity [54]. The classification of adsorption isotherms is characteristic of adsorbents that are microporous (type I), nonporous or macroporous (types II, III, and VI), or mesoporous (types IV and V). The result of nitrogen adsorption/desorption isotherms of GO/CS granular adsorbent in this study at 77 K has a shape of type V with pore diameter of 35.201 Å, indicating that the adsorbent is a mesoporous material [54,55]. Type V implies that the adsorbents possess a certain pore with a slit shape, as well as the adsorbate-adsorbent interaction is weak [54]. This description is in good agreement with the observation based on FE-SEM images of GO/CS granular adsorbent. Moreover, with the mesoporous structure, the GO/CS granular adsorbent in this study can adsorb MB molecules easily because the size of MB molecules is about 14.2 Å in length and about 9.5 Å in width [56]. Finally, the above findings suggest that the adsorption of MB onto GO/CS adsorbent may be a weak interaction and mostly happens in the particle's inner.

3.1.5. Point of zero charge of GO/CS adsorbent

The pH of the point of zero charge (pH_{pzc}) is a critical parameter that gives an idea to understand the surface chemistry of an adsorbent. It is one of the essential physicochemical parameters indicating the net charge of an adsorbent when it comes in contact with water [57]. The pH_{pzc} is defined as the pH of the solution at which the surface charge of the adsorbent has zero value. The global

surface charge of the adsorbent is negative at pH higher than pH_{pzc} (i.e., pH > pH_{pzc}) and positive at pH lower than pH_{pzc} (i.e., pH < pH_{pzc}). Published reports revealed that adsorption of cationic dye occurs at pH > pH_{pzc} due to the existence of some functional groups, such as COO^- and OH^- [58]. In this work, pH_{pzc} was determined by the salt addition method [37] and the pH_{pzc} of GO/CS adsorbent was calculated to be 8.02 ± 0.02 as shown in Fig. 6. This signifies that at pH < pH_{pzc}, the adsorbent surface carries positive charge and at pH > pH_{pzc}, the negative charge exists on the adsorbent surface. In other words, the cationic dye (MB) in this study may be strongly adsorbed by GO/CS adsorbent at pH greater than pH_{pzc} 8.02 ± 0.02.

3.2. MB adsorption studies

3.2.1. Effect of the CS solution and reaction time in glutaraldehyde solution on MB adsorption efficiency

The GO/CS granular adsorbent in this study was synthesized via self-assembly method with effect of two parameters, including concentration of CS solution and cross-linking reaction time. To evaluate the optimum condition for the adsorbent synthesis, the comparison of MB adsorption efficiency at every condition was conducted and the results were shown in Fig. 7. As can be seen from Fig. 7, the MB adsorption efficiency of the GO/CS granular adsorbent decreased as the amount of chitosan added and reaction time in glutaraldehyde solution increased. This may be interpreted as follows as the chitosan content rose, the total surface area of the GO/CS granular adsorbent decreased due to the fact that chitosan covered more the surface of GO leading to reduce the number of functional groups on the surface of GO as well as pore diameter of the adsorbent [59]. Furthermore, as the reaction time with glutaraldehyde increased, the MB adsorption capacity decreased due to the impact of cross-linking creation. The extensive cross-linking decreased the pore size and porous structure of the adsorbent, preventing the diffusion of MB molecules to the surface of adsorbent resulting in decrease of MB adsorption efficiency [60]. Thoroughly the evaluation of the MB adsorption capacity of GO/CS granular adsorbent with different chitosan contents and the time required for the reaction in glutaraldehyde solution, the GO/CS granular adsorbent synthesized via a CS solution 1.5% and the reaction time in glutaraldehyde solution of 2 h was selected for further adsorption studies.

3.2.2. Effect of critical factors on MB adsorption

Adsorption of dyes are affected by several factors, and solution pH is one of the most important factors because of its impact on both the active sites of the adsorbent and the ionization process of the dye molecules in the solution [61]. The effect of solution pH on the adsorption process of MB is shown in Fig. 8a. When the pH increased from 4 to 6, the MB adsorption capacity slightly increased from 67.15 ± 0.04 mg/g to 70.86 ± 0.05 mg/g due to similarity in surface charge of adsorbent and the molecular charge of MB. At a low pH environment, there were plenty of protons competing with cationic MB for the same adsorption site on the adsorbent, resulting in steric hindrance. In the meantime, these protons promote the protonation of amine groups of the adsorbent to form NH_2^+ groups. This also caused an electrostatic repulsion with positively charged MB ions. According to the point of zero charge (pH_{pzc} 8.02 ± 0.02) shown in Fig. 5, the predominant functional groups of the adsorbent surface were positive at pH < pH_{pzc}; hence, in acidic condition, the hydrophilic adsorption via hydrogen bonding became dominant in the adsorption mechanism [61]. When the pH was greater than 6.0, the adsorption capacity was relatively high. When the pH varied from 6.0 to 8.0, the adsorption capacity increased to 73.44 ± 0.01 mg/g. If further changed to pH 9.0 and 10, the adsorption capacity increased by about 4 mg/g to around 77.5 ± 0.02 mg/g. At this pH range, the GO/CS material could be deprotonated, enhancing its electrostatic attraction with MB ions, thereby accelerating its adsorption capacity [62]. Therefore, to carry out further studies, pH 8.0 was considered as an optimum value.

To evaluate adsorption rate, the effect of the contact time on adsorption capacity was conducted and the results were depicted in Fig. 8c. As can be seen from Fig. 8c, the adsorption capacity rose sharply from 22.53 ± 0.04 mg/g at the first 30 min to 73.23 ± 0.03

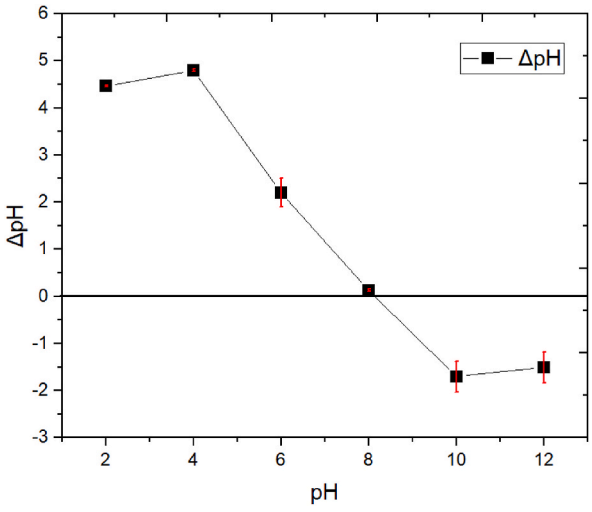

Fig. 6. Point of zero charge of GO/CS granular adsorbent.

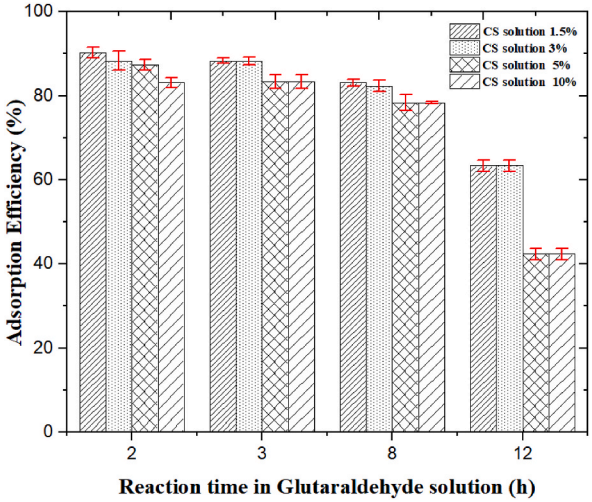

Fig. 7. Effect of the CS solution and reaction time in glutaraldehyde solution on MB adsorption efficiency. C_{MB} = 20 mg/L, $m_{CO/CS}$ = 5 mg, V = 40 mL, t = 24 h, pH = 8.0, T = 303K

mg/g at 4 h. This may be explained by the fact that at first cationic dyes adsorbed onto the outer surface of the granular adsorbent, then they diffused from the surface to inner parts of the granular adsorbent. Herein, many surface active sites were accessible for adsorption of MB on the surface of GO/CS granular adsorbent [63,64]. After 4 h, the adsorption capacity increased slightly as time went on; thus, the growth rate became less noticeable, and it gradually got close to the adsorption equilibrium after 24 h. Indeed, the adsorption capacity was only enhanced from 73.23 ± 0.02 mg/g at 4 h to 76.64 ± 0.03 mg/g at 24 h. For adsorption efficiency, it just rose from 91.54% to 95.79% when the contact time extended from 4 h to 24 h. This insignificant efficiency within a very long time adsorption was attributed to saturation of surface active sites [64]. Besides, adsorbent used in this study was a granular form, so MB ions had to take more time to diffuse from bulk solution to central granule. Moreover, after the first 4 h, the concentration of MB ions was low, causing a decrease in gradient concentration between bulk solution and inner part of granule [65]. Therefore, the subsequent tests were conducted with contact time of 4 h.

Besides pH and contact time, initial concentration plays an essential role in the adsorption process. This study evaluated the effect of initial MB concentration on MB adsorption using GO/CS granular adsorbent, and presented in Fig. 8b. In general, both adsorption efficiency and adsorption capacity increased with increasing MB concentration. However, adsorption efficiency moderately rose from 85.68 ± 0.03% to 98.67 ± 0.01% when initial MB concentration went from 5 mg/L to 40 mg/L. In the meantime, adsorption capacity went almost linearly from 37.23 ± 0.03 mg/g to 295.09 ± 0.04 mg/g at the identical concentration range. At the low concentration, there were much more active sites on the surface of adsorbent compared to the adsorbate; hence, although more than 85% of MB was adsorbed, the adsorption capacity was just 37.23 ± 0.03 mg/g. When initial concentration of MB stepwise rose to 40 mg/L, the adsorption capacity increased corresponding to 295.09 ± 0.04 mg/g. This increase was attributed to the fact that the concentration of dye molecules outside of the GO/CS granules was much greater than the concentration inside the GO/CS granules, causing a strongly chemical driving force to enhance diffusion of MB ions into the granular adsorbent [64,65]. Moreover, due to the increasing concentration gradient, the dye molecules diffused into the GO/CS granules, increasing the osmotic pressure inside the granules and causing the swelling of GO/CS granules [65]. This allows MB ions to diffuse deeper into central regions of the adsorbent.

In contrast to initial concentration, increase in adsorption dose causes a growth-up of adsorption efficiency, but a reduction of adsorption capacity. In this study, the effect of adsorption dose was conducted in a range of 5–50 mg, and shown in Fig. 8d. When the quantity of adsorbent rose from 5 mg to 10 mg, the MB adsorption efficiency improved fast from 82.41 ± 0.02% to 97.69 ± 0.03% due to increase of surface active sites of the adsorbent. However, the adsorption efficiency mostly remained unchanged when the adsorbent dosage continued to increase to 50 mg, attributing to constant of MB concentration. For adsorption capacity, it went down fast from 82.41 ± 0.02 mg/g to 23.79 ± 0.03 mg/g as the adsorption dose varied from 5 mg to 50 mg. This fall is due to the fact that adsorption capacity was inversely proportional to the adsorbent amount [66].

In this work, the temperature effect on MB adsorption using GO/CS granular adsorbent was assessed and presented in Fig. 8e. The adsorption effectiveness decreased as the temperature rose from 303 K to 333 K. This observation is in good agreement with the adsorption of MB using sulfuric acid-treated orange peel [67]. The results show that the adsorption of MB onto GO/CS granular adsorbent is exothermic in nature. The decrease in the MB adsorption efficiency with increase in temperature may be due to weakening of the adsorptive forces between the MB molecules and the active sites of GO/CS granular adsorbent [68]. Moreover, high temperatures enhanced the solubility of MB and reduced attractive forces between the adjacent molecules of the adsorbed phases. This caused an increase in desorption rate or decrease in the adsorption capacity [65].

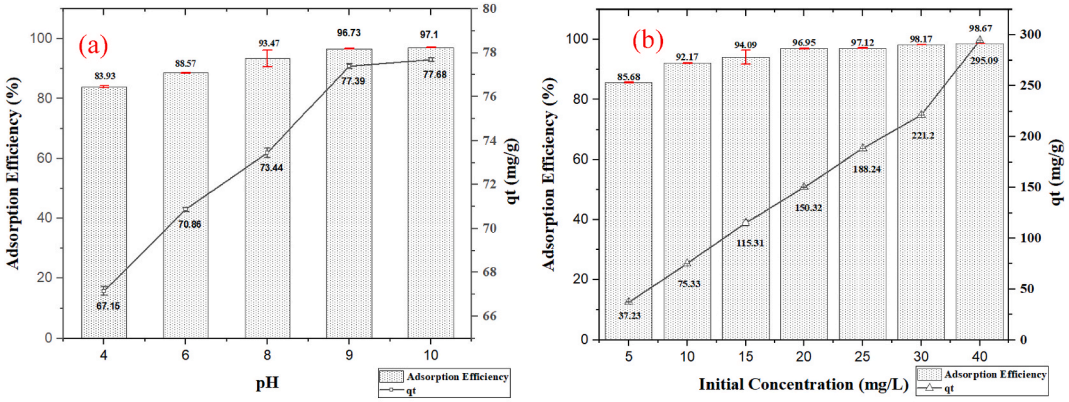

(a): $m_{GO/CS}$=10 mg, V=40 mL, C_{MB}=20 mg/L, t=6 h; (b): $m_{GO/CS}$=10 mg, V=40 mL, t=6 h, pH=8.0

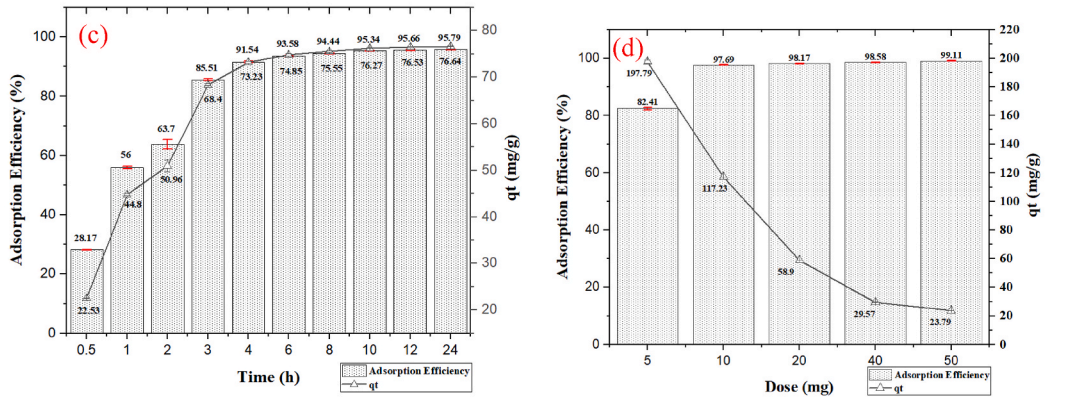

(c): $m_{GO/CS}$=10 mg, V=40 mL, C_{MB}=20 mg/L, pH=8.0; (d): C_{MB}=20 mg/L, V=40 mL, t=4 h, pH=8.0

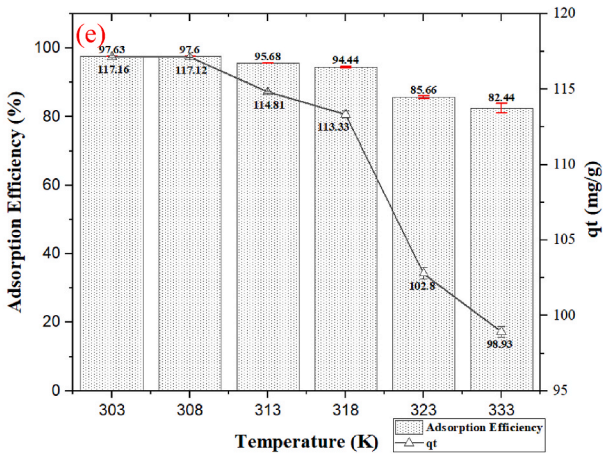

(e): C_{MB}=20 mg/L, $m_{GO/CS}$=10 mg, V=40 mL, t=4 h, pH=8.0

Fig. 8. Effect of pH (a), initial concentration (b), contact time (c), adsorbent dose (d), and temperature (e) on MB adsorption by GO/CS adsorbent.

3.3. Adsorption kinetics

Kinetic equations are applied to determine the adsorption mechanism providing useful data to enhance the adsorption capacity and practicability of scale-up. In this work, the mechanism of MB adsorption using GO/CS adsorbent was investigated by fitting PFO and PSO to the experimental data. The results were presented in Fig. 9a and the important parameters were shown in Table 2. The data obtained for MB adsorption using GO/SC adsorbent show that the adsorption kinetics were well fitted to the PSO model because of the

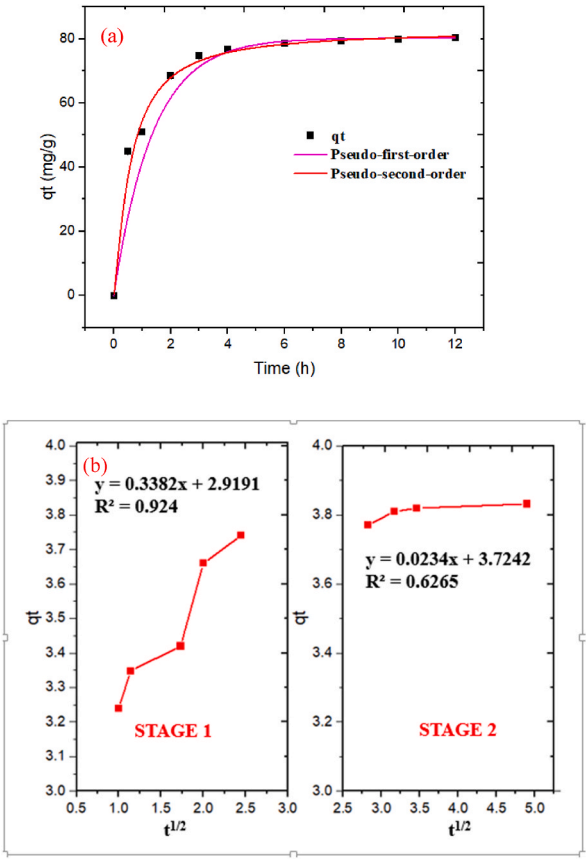

Fig. 9. Pseudo-first-order model and Pseudo-second-order model (a), Intra-particle diffusion model (b) for MB adsorption by GO/CS adsorbent.

Table 2
Kinetic parameters and coefficients of PFO and PSO model.

Kinetic model	Parameters	Definition	Values
pseudo-first-order	q_e, cal (mg/g)	Calculated adsorption capacity	157.61 ± 0.03
	k_1	Rate constant	−0.18 ± 0.01
	R^2	Correlation coefficient	0.989
	SSE	Sum of the squares of the errors	1.474
pseudo-second-order	q_e, cal (mg/g)	Calculated adsorption capacity	179.65 ± 0.03
	k_2	Rate constant	0.11 ± 0.02
	R^2	Correlation coefficient	0.999
	SSE	Sum of the squares of the errors	1.054

Table 3
Intra-particle diffusion model of Adsorption of MB on GO/Chitosan.

Kinetic model	Parameters	Definition	Values
Stage 1	k_{p1}(mg/g.min$^{1/2}$)	Rate constant at stage 1	0.3382
	C_1	Intercept at stage 1	2.9191
	Ri_1	The initial adsorption	0.2437
	R^2	Correlation coefficient	0.924
	C/q_{ref}		0.7805
	Zone		III
Stage 2	k_{p2}(mg/g.min$^{1/2}$)	Rate constant at stage 2	0.0234
	C_2	Intercept at stage 2	3.7242
	Ri_2	The initial adsorption	0.0297
	R^2	Correlation coefficient	0.6265
	C/q_{ref}		0.971
	Zone		IV

goodness of fit R^2 highly closing to 1. The applicability of PSO model to describe the kinetics of MB adsorption were also reported by Kumar et al. (2014) [67] using sulfuric acid-treated orange peel and Jia et al. (2018) [56] using bone char.

Moreover, Table 2 shows that the obtained calculated q_e (179.65 ± 0.03 mg/g) was consistent with the obtained experimental q_e (150,32 ± 0.03 mg/g). It can be seen from Table 2, the slope of the quadratic symbolic equation, a = 0.25, was compatible with the stated item MB adsorption capacity. According to Fig. 9a, dependability grew fast as the slope of the tiny slope increased. The lower the slope coefficients, the lower the t/q_t. Because q_t is inversely proportional to t/q_t, a slight slope will enhance data processing speed in MB.

In this work, the adsorbent is granules, so it is necessary to employ an intra-particle diffusion model to study. Fig. 9b and Table 3 described the application of the intra-particle diffusion model to MB adsorption using GO/CS granular adsorbent. It can be seen in Fig. 9b, in the first stage, the slope of the straight line was sharp, and the slope was large $k_{p1=}0.3382$ (mg/g.$min^{1/2}$), indicating the fast outer surface adsorption of the adsorbent boundary layer diffusion [31,68]. The values of Ri_1 and C/q_{ref} obtained for the adsorption of MB on GO/CS obtained in the initial adsorption were respectively 0.2437 and 0.7805. These values show that they belonged to zone 3, indicating a strongly initial adsorption of MB on GO/CS granular adsorbent. This statement is in good agreement with the result of contact time effect on adsorption capacity in Fig. 8c.

The slope of the second stage k_{p2} = 0.0234 (mg/g.$min^{1/2}$) decreased and corresponded to the adsorption generated by intra-granular diffusion; this is progressive adsorption. The values of Ri_2 = 0.0297, C/q_{ref} = 0.971 in Table 3 showed the initial adsorption belonging to zone 4. In other words, the initial adsorption of MB onto the surface of GO/CS granular adsorbent was approaching completely initial adsorption or the initial adsorption took into account for more than 90% of the adsorption process [31]. Fig. 9b also shows that the two linear fitting straight lines did not pass the origin point to indicate that the adsorption of MB by GO/CS granular adsorbent, in addition to the particle diffusion rate control, could be controlled by other steps [63].

3.4. Adsorption isotherms

Adsorption isotherms are frequently applied to assess the adsorption capacity of adsorbents. These models describe adsorbent and adsorbate interaction, as well as the surface properties of adsorbent [36]. The experimental data in this work was fitted to two common adsorption isotherm models, including the Langmuir and Freundlich model. According to Eq. (10), the nonlinear Langmuir model was shown in Fig. 10a and the Langmuir constants k_L (L/g) and q_{max} (mg/g) were listed in Table 4. As can be seen from Table 3, the adsorbent had the maximum adsorption capacity of 951.35 ± 0.03 mg/g at 303 K with R^2 = 0.974. However, the regression coefficient is a little far from 1, so the experimental data in this study are not totally fitted to the Langmuir adsorption isotherm.

The Freundlich model simulates multilayer coverage on the surface of the adsorbent as well as surface heterogeneity [32]. In this study, Fig. 10b shows the nonlinear Freundlich model and Table 4 tabulates the obtained isotherm constants and coefficients which were calculated from the linearized model. Table 4 indicates that the regression coefficient, R^2 = 0.997, was high and could state that the MB adsorption by GO/CS adsorbent was more consistent with the Freundlich model than the Langmuir model. For the Freundlich model, when n = 1.117 or 1/n = 0.895, the adsorption process was favorable because the slope of the straight line was low. The adsorption of MB on the surface of GO/CS adsorbent was also reversible with different adsorption energy between adsorbate and adsorbent as well as the adsorbent could adsorb multilayer of MB on its surface [69].

Table 4 lists adsorption systems of MB fitted with the R–P isotherm equation. Large molecule adsorption, as in dyes, is not easy in accordance with the theory of monolayer adsorption upon which the Langmuir isotherm equation is based [35]. This is because impediments exist between pores and adsorbate so the β value is usually less than 1 [70]. Subramani et al. also reported that when studying the R–P isotherm model when using Chitosan beads to adsorb dye, the value β is also less than 1 [71].

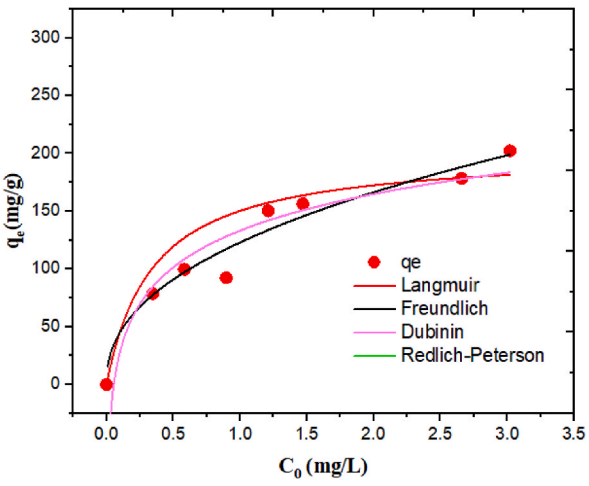

Fig. 10. Langmuir, Freundlich,Dubinin- Radushkevich Non-linear isotherm for MB adsorption on GO/CS granular adsorbent.

Table 4
Isotherm parameters and coefficients of Langmuir, Freundlich, and Dubinin Radushkevich model of MB adsorption using GO/CS adsorbent.

Adsorption isotherm	Parameters	Values
Langmuir	q_{max} (mg/g)	951.35 ± 0.03
	k_L (L/mg)	0.298 ± 0.02
	R^2	0.974
	SSE	1.124
Freundlich	k_F (L/mg)	4.157 ± 0.04
	1/n	0.895
	R^2	0.997
	SSE	1.087
Dubinin- Radushkevich	E (kJ/mol)	0.98 ± 0.03
	R^2	0.996
	SSE	1.278
Redlich-Peterson	K_{rp}	2.531
	β a	0.964
	R^2	0.053
	SSE	0.995
		1.167

To investigate the adsorption free energy and characteristic porosity, the Dubinin-Radushkevich (D-R) model is applied [27]. Besides these two characteristics, one of the unique features of the D-R isotherm model is temperature dependent, indicating the non-homogeneous surface of the adsorbent [38]. This study used Eq. (12) linearized to Eq. (13) to plot D-R graph in Fig. 10. From the linear plot of D-R model, the mean free energy was determined to be E = 0.98 ± 0.03 kJ/mol (Table 4). The value of E was valuable for appraising the type of adsorption process. When E < 8.0 kJ/mol, the adsorption type can be described by physical adsorption [34]. In this study, the value of E is 0.98 ± 0.03 kJ/mol, suggesting that the adsorption process of MB onto adsorbent is monolayer to be physical in nature. However, the regression coefficient (R^2) of D-R model in this study is 0.996, indicating that the experimental data partially agreed with the D-R model. Finally, the adsorption of MB onto the surface of GO/CS granular adsorbent was well described by the Freundlich adsorption isotherm model.

3.5. Thermodynamic study

The critical thermodynamic parameters such as Gibbs free energy, enthalpy and entropy change are determined via evaluation of the temperature effect on MB adsorption by GO/CS adsorbent [37]. The influence of these parameters on MB adsorption was determined based on Eq. (16) and Eq. (17), and the results were presented in both Fig. 11 and Table 5. The above mentioned parameters were obtained by drawing a fitted straight line graph of ln(K_C) relative to 1/T. It can be seen from Fig. 11 that the adsorption capacity of the GO/CS for MB decreased with increasing temperature. Table 5 shows that the Gibbs free energy (ΔG^0) for MB adsorption was negative at all temperatures, indicating that the adsorption of MB by the GO/CS was spontaneous and thermodynamically favorable. As can be seen that the value of Gibbs free energy varied from −11.7 ± 0.01 (kJ/mol) to −3.12 ± 0.02 (kJ/mol) when the temperature increased from 303 to 333 K, which pointed out that the adsorption of MB on GO/CS adsorbent at lower temperature was more spontaneous. The negative change of enthalpy ΔH^0 = −98.358 ± 0.03 (kJ/mol) indicated that the adsorption of MB by the GO/CS

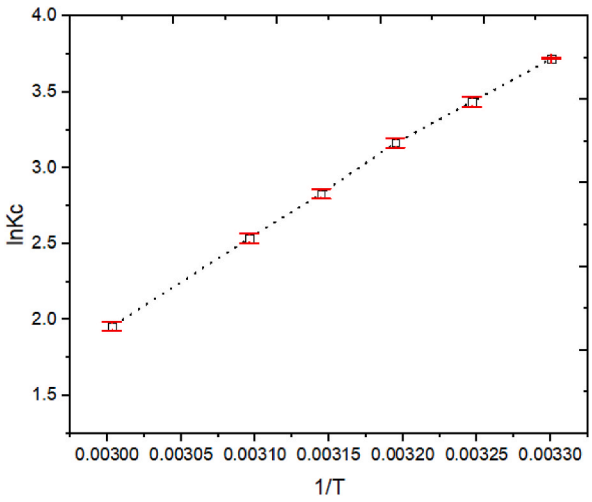

Fig. 11. Van't Hoff plot for the adsorption of MB on GO/CS adsorbent.

Table 5
Thermodynamic Parameters for MB adsorption on GO/CS adsorbent.

T (K)	ΔG^0 (kJ/mol)	ΔH^0 (kJ/mol)	ΔS^0 (J/mol K)
303	−11.7 ± 0.01	−98.358 ± 0.03	−0.286 ± 0.04
308	−10.27 ± 0.02		
313	−8.84 ± 0.03		
318	−7.41 ± 0.04		
323	−5.98 ± 0.01		
333	−3.12 ± 0.02		

granules was an exothermic process, which was in good agreement with the results obtained from the study of Othman et al. (2020) using alginate-based beads to adsorb methylene blue from water [72] and Durrani et al. (2022) using palm based activated carbon-alginate membrane to adsorb MB from aqueous solution [73]. However, it is interesting that several articles have been reported an endothermic process of MB ions adsorption onto different biomass based adsorbent such as cellulosic olive stones [63], activated carbon developed from *Ficus Carica* bast [74], or peat [75]. The negative value of entropy change (ΔS^0) states that the randomness on the granule-MB interface was reduced. In other words, MB ions were condensed on the surface of the adsorbent [76,77].

The mechanism of adsorption mainly depends upon morphology properties and chemistry of both adsorbent and adsorbate [37]. In this study, the main mechanism of MB adsorption onto GO/CS granular adsorbent was depicted in Fig. 12. According to the electrical characteristics of GO/CS adsorbent and MB following hydrolysis, both include carboxyl groups and benzene rings. It is hypothesized that MB adsorption on GO/CS surface could be attributed to the following three forces such as an electrostatic attraction between the GO/CS and MB molecules, establishment of hydrogen bonds of carboxyl groups of GO/CS with MB and a stacking action between the benzene rings of GO/CS and MB [78].

3.6. Desorption of MB

3.6.1. Effect of solvent, contact time, and temperature on MB desorption

Reusing the spent adsorbents are considered as an essential aspect in reducing economic consumption [74]. To evaluate the recycling of adsorbents, it is necessary to conduct a desorption process to understand the mechanism of the adsorbed MB on the GO/CS granules. For desorption, solvents are critical to evaluate releasing ability of adsorbate [79]. As a sustainable development approach, this study used three solvents including sodium chloride solution 1 M, ethanol 70% and DI water in order not to produce hazardous leachates and the results were presented in Fig. 13a. Sodium chloride solution 1 M had a desorption efficiency of 72.85 ± 0.03% and a release capacity of 85.4 ± 0.04 mg/g while the desorption efficiency of using ethanol was 82.68 ± 0.03% and the desorption capacity was of 96.92 ± 0.02 mg/g. Thus, ethanol had a favorable effect to release MB compared to sodium chloride, similar result is found in study of Daneshvar et al. (2017) using sodium chloride and ethanol for desorption of MB from brown macroalga [79]. The lower desorption capacity of using sodium chloride solution 1 M may be due to the fact that huge amount of Cl^- ion from NaCl could increase the anionic characteristics of GO/CS adsorbent and give it a more favorable and stronger electrostatic interaction with the cationic MB, preventing the MB desorption from the spent GO/CS adsorbent. Meanwhile, the solvent's polarity, solubility of MB in ethanol, and the ease of penetration to the pores were attributed to successful release of MB into ethanol [80]. Fig. 13a also shows that when using DI water, the desorption efficiency and desorption capacity were 80.46 ± 0.05% and 94.32 ± 0.04 mg/g, respectively, being lower compared to using ethanol. The reason could be that the polarity of the DI water solvent is relatively high compared to that of ethanol. Moreover, surface tension of water at 323 K is 68.45×10^3 N/m while surface tension of ethanol 70% is 22.15×10^3 N/m at the same temperature [81]. This allows ethanol 70% dispersed deeply and faster into GO/CS granules, accelerating the desorption process of MB. However, the desorption efficiency of using DI water was not much lower than that of using ethanol 70%, and using chemical reagents like sodium chloride and ethanol could produce potentially hazardous leachates compared to using DI water [82]. Therefore, the desorption solvent for further experiments was DI water.

Besides solvents, contact time is an influencer acting on the desorption process of MB. The effect of contact time on MB desorption was conducted and shown in Fig. 13b. It can be seen that as the reaction time lengthened, desorption efficiency increased. The desorption capacity gradually increased from 48.84 ± 0.04 mg/g up to 104.44 ± 0.05 mg/g, and the desorption capacity rate increased rapidly within the first 4 h, and then slowed down the rate for the last 3 h. This could be caused by the fact that when the dye was released more into bulk solution, the concentration gradient reduced the driving force of the dye diffusion from inner granule to bulk solution [30]. Moreover, as time went on, the backward reaction rate increased and caused an increase in the re-adsorption process of MB onto the solid surface. In other words, reducing dye concentration in the solid phase and solvent saturation may be responsible for slowing down dye desorption rate.

In the desorption process, temperature is one of important factors playing a significant role in dyes desorption [83]. Therefore, in this study MB desorption process was conducted in temperature change ranging from 313 to 353 K and the results were shown in Fig. 13c. The desorption efficiency increased from 45.45 ± 0.01% to 92.88 ± 0.04% or the desorption capacity rose from 53.28 ± 0.04 mg/g to 108.88 ± 0.01 mg/g when the temperature varied from 313 to 333K. However, MB desorption efficiency reduced as the temperature further improved. According to the adsorption experiment data in this study, adsorption was inhibited by rising temperature or following the thermodynamic study, the adsorption process of MB onto GO/CS adsorbent was exothermic. These findings imply that the desorption capacity rose as heating up the effluent. Moreover, according to Momina et al. (2020), increasing

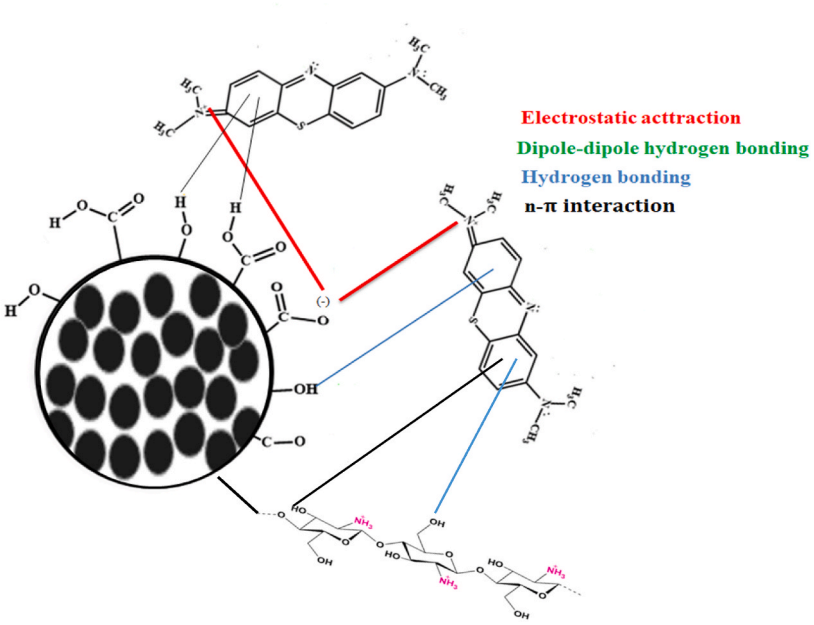

Fig. 12. Adsorption mechanism of MB on GO/CS granular adsorbent.

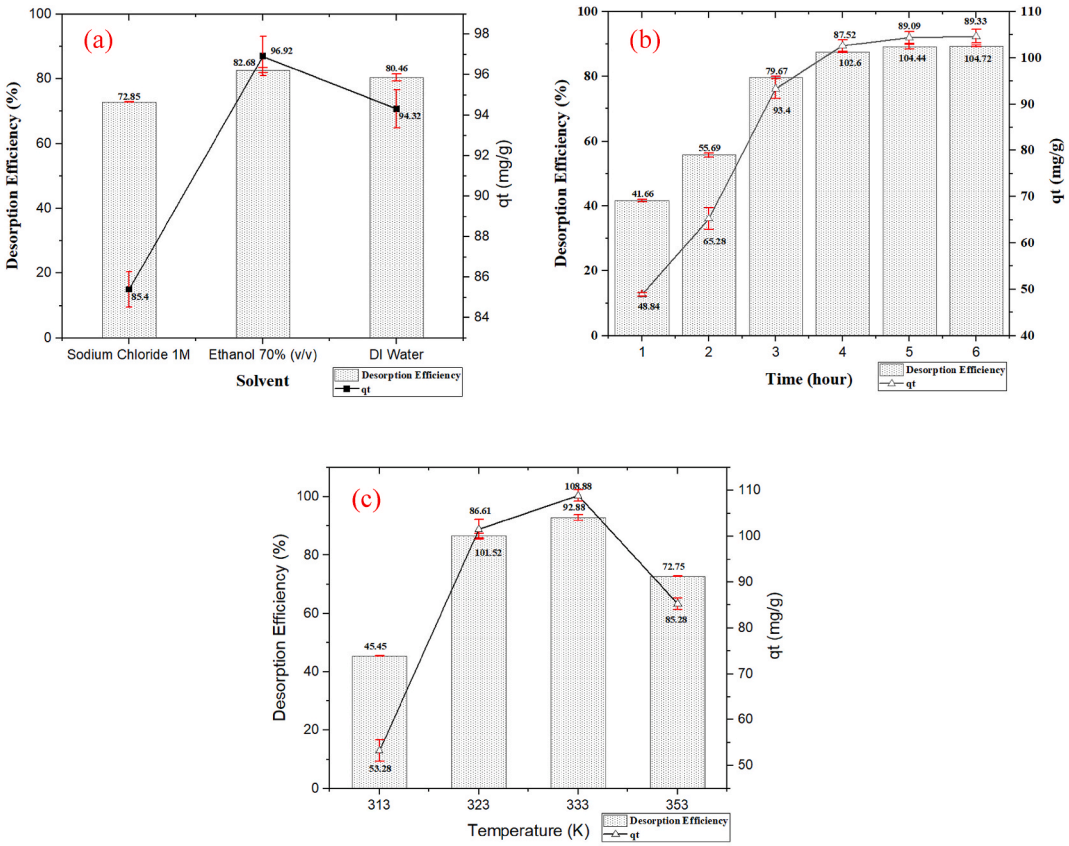

(a) t=4 h, T=323 K; (b): solvent=DI water, T=323 K;(c): solvent=DI water, t=4 h

Fig. 13. Effect of (a) solvent, (b) contact time, (c) temperature on MB desorption with ultrasound applied.

temperature could make an enhancement in desorption efficiency up to a certain limitation, further increasing temperature, however, resulted in an inactive desorption because MB molecules diffuse more onto solid phase [83].

3.6.2. Lifespan of adsorbent

The goal of regenerative research is to establish the material's adsorption capacity after a number of successive adsorption/desorption cycles [83]. Utilizing DI water as the solvent and ultrasound in combination with heat, several adsorption/desorption cycles were carried out up to seven times and the performance was depicted in Fig. 14.

In general, the MB adsorption efficiency of GO/CS adsorbent decreased from 97.32% of the first cycle to 58% of the seventh cycle. However, desorption efficiency remained almost unchanged after seven cycles at a value of 91.08%. This decrease might be due to the fact that active sites on the surface of the adsorbent were saturated, causing a decrease in adsorbent's surface area and leading to the reduction in adsorption effectiveness [83]. Additionally, the GO/CS granular adsorbent was broken down after seven cycles of working because the adsorbent worked under high temperature associated with ultrasonic application for a long time, causing a break in its structure. Because the mechanism of synthesizing GO/CS material is the electrostatic interaction between the amino group (NH_2), primary and secondary hydroxyl groups (CH_2OH, CHOH) of chitosan and the surface of the carboxyl group (COOH) and the hydroxyl (OH) on GO, combined with the cross-linking of Chitosan and glutaraldehyde. When materials worked under high temperature conditions combined with ultrasonic waves and for long periods of time, these bonds were degraded by ultrasonic waves and temperature [84,85]. Therefore, these GO/CS granules could not be retrieved.

3.7. Comparison with other GO-based adsorbents

The adsorption capacity of GO/CS material for adsorption of MB is compared with other GO-based adsorbents reported in previous studies. The calculated maximum adsorption capacity of GO/CS material was 951.35 mg/g, which was mostly higher than the adsorption capacities of GO-based adsorbents as shown in Table 6. The first group using magnetic combined with cellulose/GO [61], with chitosan/GO [87] or with GO/sodium alginate [88] to adsorb MB with the calculated q_{max} was 70, 180.8 or 317 mg/g, respectively. In the meantime, when GO combined with casein or $CoFe_2O_4$, the computed q_{max} was quite high with the value of 437.29 [63] and 355.9 mg/g [89]. However, when GO went with chitosan and carboxymethyl cellulose, the calculated maximum adsorption capacity was significantly improved and got the highest value of 3190 mg/g [90]. Another study in 2018 conducted by Qi et al. used GO combined with chitosan to produce a sponge to remove MB in aqueous solution [86], the result showed that the computed q_{max} was 180.8 mg/g, which was lower the calculated q_{max} of this study (951.35 mg/g). This could be caused by high chitosan content used (9%) in their study compared to 1.5% content of chitosan used in this study. The above findings suggest that GO/CS granules may be used as an excellent adsorbent for the removal of MB from aqueous solution due to the presence of different oxygen functional groups, mesoporous structure and high adsorption capacity.

4. Conclusion

In this study, the granular adsorbent was successfully synthesized using self-assembly with glutaraldehyde as a cross-linker. The as-synthesized adsorbent had a diameter of 1.05 ± 0.04 mm with specific surface area of 1.235 m^2/g and possessed mesoporous structure with pore diameter of 35.201 Å as well as pH_{pzc} of 8.02 ± 0.02. Fourier transform infrared analysis confirmed the formation of covalent bonds between graphene oxide and chitosan after cross-linking with glutaraldehyde. The optimal adsorption capacity (117.16 ± 0.03 mg/g) was obtained at pH 8.0 with initial concentration of 20 mg/L, adsorbent dose of 10 mg, contact time of 4 h, adsorption

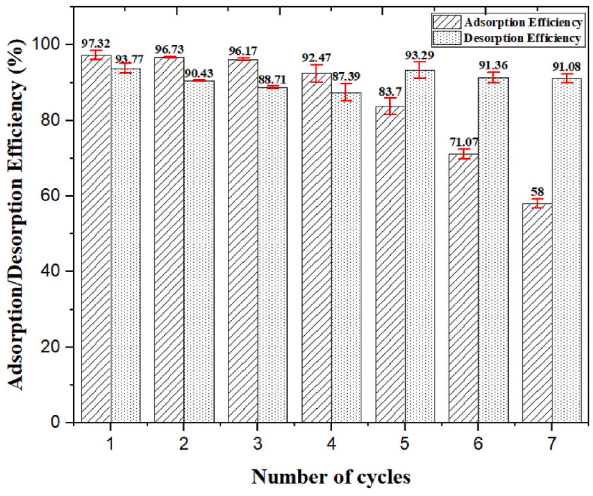

Fig. 14. Regeneration of GO/CS granular adsorbent (solvent: DI water, t: 4 h, T: 333 K, ultrasound applied).

Table 6
Comparison adsorption capacities of MB by GO/CS with other GO-based adsorbents.

Adsorbent	Calculated q_{max} (mg/g)	References
Magnetic cellulose/GO composite	70	[61]
CA/GO	437.29	[63]
GO/CS sponge (CS 9%)	275.5	[86]
Magnetic chitosan GO	180.8	[82]
Fe_3O_4@GO@SA	317	[83]
$CoFe_2O_4$/GO	355.9	[84]
CS-GO/CMC-1/1	3190	[85]
GO/CS granular adsorbent	951.35	In this study

temperature of 303 K. The adsorption kinetic showed a good agreement between the pseudo-second-order model and experimental data while adsorption isotherm of dye onto the adsorbent was consistent with Freundlich model. The physical forces are the main mechanism of dye adsorption by using the granular adsorbent. The intra-particle diffusion model confirmed that dye adsorption in this work was also mostly happened within the first stage of adsorption. The thermodynamic study determined dye adsorption using the granular adsorbent was a spontaneous and exothermic process and dye molecules condensed onto the adsorbent. Furthermore, the desorption conducted by DI water at 333 K combined with ultrasound showed a 6-time reuse of the adsorbent in this investigation. Therefore, the granular adsorbent has a great potential to be applied for wastewater treatment of methylene blue or other cationic dyes in the near future.

Data availability

Data included in article/supp. material/referenced in article.

CRediT authorship contribution statement

Huynh Vu Thanh Luong: Writing – review & editing, Writing – original draft, Supervision, Resources, Conceptualization. **Thanh Phu Le:** Writing – original draft, Methodology, Investigation, Data curation. **Tran Lan Trinh Le:** Methodology, Data curation. **Huynh Giao Dang:** Writing – review & editing. **Thi Bich Quyen Tran:** Writing – review & editing.

Declaration of competing interest

None.

Acknowledgments

None.

References

[1] K.C. Jones, Persistent organic pollutants (POPs) and related chemicals in the global environment: some personal reflections, Environ. Sci. Technol. 55 (2021) 9400–9412, https://doi.org/10.1021/acs.est.0c08093.
[2] F. Mashkoor, A. Nasar, Magsorbents: potential candidates in wastewater treatment technology–A review on the removal of methylene blue dye, J. Magn. Magn Mater. 500 (2020) 166408, https://doi.org/10.1016/j.jmmm.2020.166408.
[3] P. Grandjean, P.J. Landrigan, Neurobehavioural effects of developmental toxicity, Lancet Neurol. 13 (2014) 330–338, https://doi.org/10.1016/S1474-4422(13)70278-3.
[4] J.-P. Desforges, A. Hall, B. McConnell, A. Rosing-Asvid, J.L. Barber, A. Brownlow, et al., Predicting global killer whale population collapse from PCB pollution, Science. 361 (2018) 1373–1376, https://doi.org/10.1126/science.aat1953.
[5] M. Shaban, M.R. Abukhadra, S.S. Ibrahim, M.G. Shahien, Photocatalytic degradation and photo-Fenton oxidation of Congo red dye pollutants in water using natural chromite—response surface optimization, Appl. Water Sci. 7 (2017) 4743–4756, https://doi.org/10.1007/s13201-017-0637-y.
[6] G. Pandey, S. Singh, G. Hitkari, Synthesis and characterization of polyvinyl pyrrolidone (PVP)-coated Fe 3 O 4 nanoparticles by chemical co-precipitation method and removal of Congo red dye by adsorption process, Int. Nano Lett. 8 (2018) 111–121, https://doi.org/10.1007/s40089-018-0234-6.
[7] G. Karthigadevi, S. Manikandan, N. Karmegam, R. Subbaiya, S. Chozhavendhan, B. Ravindran, et al., Chemico-nanotreatment methods for the removal of persistent organic pollutants and xenobiotics in water–A review, Bioresour. Technol. 324 (2021) 124678, https://doi.org/10.1016/j.biortech.2021.124678.
[8] R. Lafi, I. Montasser, A. Hafiane, Adsorption of Congo red dye from aqueous solutions by prepared activated carbon with oxygen-containing functional groups and its regeneration, Adsorpt. Sci. Technol. 37 (2019) 160–181, https://doi.org/10.1177/0263617418819227.
[9] N. Rao, R. Singh, L. Bashambu, Carbon-based nanomaterials: synthesis and prospective applications, Mater. Today: Proc. 44 (2021) 608–614, https://doi.org/10.1016/j.matpr.2020.10.593.
[10] R. Thines, N. Mubarak, S. Nizamuddin, J. Sahu, E. Abdullah, P. Ganesan, Application potential of carbon nanomaterials in water and wastewater treatment: a review, J. Taiwan Inst. Chem. Eng. 72 (2017) 116–133, https://doi.org/10.1016/j.jtice.2017.01.018.
[11] T. Kuilla, S. Bhadra, D. Yao, N.H. Kim, S. Bose, J.H. Lee, Recent advances in graphene based polymer composites, Prog. Polym. Sci. 35 (2010) 1350–1375, https://doi.org/10.1016/j.progpolymsci.2010.07.005.
[12] A.T. Smith, A.M. LaChance, S. Zeng, B. Liu, L. Sun, Synthesis, properties, and applications of graphene oxide/reduced graphene oxide and their nanocomposites, Nano Materials Science 1 (2019) 31–47, https://doi.org/10.1016/j.nanoms.2019.02.004.
[13] I. Chowdhury, M.C. Duch, N.D. Mansukhani, M.C. Hersam, D. Bouchard, Colloidal properties and stability of graphene oxide nanomaterials in the aquatic environment, Environ. Sci. Technol. 47 (2013) 6288–6296, https://doi.org/10.1021/es400483k.

[14] S. Bano, A. Mahmood, S.-J. Kim, K.-H. Lee, Graphene oxide modified polyamide nanofiltration membrane with improved flux and antifouling properties, J. Mater. Chem. A 3 (2015) 2065–2071, https://doi.org/10.1039/C4TA03607G.
[15] J. Abraham, K.S. Vasu, C.D. Williams, K. Gopinadhan, Y. Su, C.T. Cherian, et al., Tunable sieving of ions using graphene oxide membranes, Nat. Nanotechnol. 12 (2017) 546–550, https://doi.org/10.1038/nnano.2017.21.
[16] C. Zhang, K. Wei, W. Zhang, Y. Bai, Y. Sun, J. Gu, Graphene oxide quantum dots incorporated into a thin film nanocomposite membrane with high flux and antifouling properties for low-pressure nanofiltration, ACS Appl. Mater. Interfaces 9 (2017) 11082–11094, https://doi.org/10.1021/acsami.6b12826.
[17] H. Shan, C. Zeng, C. Zhao, H. Zhan, Iron oxides decorated graphene oxide/chitosan composite beads for enhanced Cr (VI) removal from aqueous solution, Int. J. Biol. Macromol. 172 (2021) 197–209, https://doi.org/10.1016/j.ijbiomac.2021.01.060.
[18] M. Bhattacharjee, A. Vilouras, R.S. Dahiya, Microdroplet-based organic vapour sensor on a disposable GO-chitosan flexible substrate, IEEE Sensor. J. 20 (2020) 7494–7502, https://doi.org/10.1109/FLEPS.2019.8792237.
[19] A. Gupta, V.S. Chauhan, N. Sankararamakrishnan, Preparation and evaluation of iron–chitosan composites for removal of as (III) and as (V) from arsenic contaminated real life groundwater, Water Res. 43 (2009) 3862–3870, https://doi.org/10.1016/j.watres.2009.05.040.
[20] L. Liu, C. Li, C. Bao, Q. Jia, P. Xiao, X. Liu, et al., Preparation and characterization of chitosan/graphene oxide composites for the adsorption of Au (III) and Pd (II), Talanta 93 (2012) 350–357, https://doi.org/10.1016/j.talanta.2012.02.051.
[21] D. Han, L. Yan, W. Chen, W. Li, Preparation of chitosan/graphene oxide composite film with enhanced mechanical strength in the wet state, Carbohydr. Polym. 83 (2011) 653–658, https://doi.org/10.1016/j.carbpol.2010.08.038.
[22] H. Zhao, T. Jiao, L. Zhang, J. Zhou, Q. Zhang, Q. Peng, et al., Preparation and adsorption capacity evaluation of graphene oxide-chitosan composite hydrogels, Sci. China Mater. 58 (2015) 811–818, https://doi.org/10.3390/gels8070447.
[23] T. Jiao, H. Zhao, J. Zhou, Q. Zhang, X. Luo, J. Hu, et al., Self-assembly reduced graphene oxide nanosheet hydrogel fabrication by anchorage of chitosan/silver and its potential efficient application toward dye degradation for wastewater treatments, ACS Sustain. Chem. Eng. 3 (2015) 3130–3139, https://doi.org/10.1021/acssuschemeng.5b00695.
[24] T.S. Vo, M.M. Hossain, T. Lim, J.W. Suk, S. Choi, K. Kim, Modification of the interfacial glass fiber surface through graphene oxide-chitosan interactions for excellent dye removal as an adsorptive membrane, J. Environ. Chem. Eng. 10 (2022) 108965, https://doi.org/10.1016/j.jece.2022.108965.
[25] R. Rashid, I. Shafiq, P. Akhter, M.J. Iqbal, M. Hussain, A state-of-the-art review on wastewater treatment techniques: the effectiveness of adsorption method, Environ. Sci. Pollut. Control Ser. 28 (2021) 9050–9066, https://doi.org/10.1007/s11356-021-12395-x.
[26] H. Zeng, Y. Yu, F. Wang, J. Zhang, D. Li, Arsenic (V) removal by granular adsorbents made from water treatment residuals materials and chitosan, Colloids Surf. A Physicochem. Eng. Asp. 585 (2020) 124036, https://doi.org/10.1016/j.colsurfa.2019.124036.
[27] N. Sharma, V. Sharma, Y. Jain, M. Kumari, R. Gupta, S. Sharma, et al., Synthesis and Characterization of Graphene Oxide (GO) and Reduced Graphene Oxide (rGO) for Gas Sensing Application, Macromolecular Symposia: Wiley Online Library, 2017 1700006, https://doi.org/10.1002/masy.201700006.
[28] M. Nasiruddin Khan, A. Sarwar, Determination of points of zero charge of natural and treated adsorbents, Surf. Rev. Lett. 14 (2007) 461–469, https://doi.org/10.1142/S0218625X07009517.
[29] H. Yuh-Shan, Citation review of Lagergren kinetic rate equation on adsorption reactions, Scientometrics 59 (2004) 171–177, https://doi.org/10.1023/B:SCIE.0000013305.99473, cf.
[30] Y.S. Ho, G. McKay, A comparison of chemisorption kinetic models applied to pollutant removal on various sorbents, Process Saf. Environ. Protect. 76 (1998) 332–340, https://doi.org/10.1205/095758298529696.
[31] F.-C. Wu, R.-L. Tseng, R.-S. Juang, Initial behavior of intraparticle diffusion model used in the description of adsorption kinetics, Chem. Eng. J. 153 (2009) 1–8, https://doi.org/10.1016/j.cej.2009.04.042.
[32] I. Langmuir, The adsorption of gases on plane surfaces of glass, mica and platinum, J. Am. Chem. Soc. 40 (1918) 1361–1403, https://doi.org/10.1021/ja02242a004.
[33] H. Freundlich, Über die adsorption in lösungen, Z. Phys. Chem. 57 (1907) 385–470, https://doi.org/10.1515/zpch-1907-5723.
[34] C. Abasi, A. Abia, J. Igwe, Adsorption of iron (III), lead (II) and cadmium (II) ions by unmodified raphia palm (Raphia hookeri) fruit endocarp, Environ. Res. J. 5 (2011) 104–113, https://doi.org/10.3923/erj.2011.104.113.
[35] F.-C. Wu, B.-L. Liu, K.-T. Wu, R.-L. Tseng, A new linear form analysis of Redlich–Peterson isotherm equation for the adsorptions of dyes, Chem. Eng. J. 162 (2010) 21–27, https://doi.org/10.1016/j.cej.2010.03.006.
[36] M. Mohammadi, A.J. Hassani, A.R. Mohamed, G.D. Najafpour, Removal of rhodamine B from aqueous solution using palm shell-based activated carbon: adsorption and kinetic studies, J. Chem. Eng. Data 55 (2010) 5777–5785, https://doi.org/10.1021/je100730a.
[37] J.S. Juma Sahar, A.N. Abdul Naeem, M.F. Muhammad Farooq, S.Z. Shah Zareen, A-u-R Ata-ur-Rahman, Thermodynamic studies of adsorption of rhodamine B and Congo red on graphene oxide (2019), https://doi.org/10.5004/dwt.2019.24436.
[38] K.Y. Foo, B.H. Hameed, Insights into the modeling of adsorption isotherm systems, Chem. Eng. J. 156 (2010) 2–10, https://doi.org/10.1016/j.cej.2009.09.013.
[39] B. Xing, C. Zhang, Y. Cao, G. Huang, Q. Liu, C. Zhang, et al., Preparation of synthetic graphite from bituminous coal as anode materials for high performance lithium-ion batteries, Fuel Process. Technol. 172 (2018) 162–171, https://doi.org/10.1016/j.fuproc.2017.12.018.
[40] J.-H. Yang, H. Yang, S. Liu, L. Mao, Microwave-assisted synthesis graphite-supported Pd nanoparticles for detection of nitrite, Sensor. Actuator. B Chem. 220 (2015) 652–658, https://doi.org/10.1016/j.snb.2015.05.118.
[41] S. Chaiyakun, N. Witit-Anun, N. Nuntawong, P. Chindaudom, S. Oaew, C. Kedkeaw, et al., Preparation and characterization of graphene oxide nanosheets, Procedia Eng. 32 (2012) 759–764, https://doi.org/10.1016/j.proeng.2012.02.009.
[42] G.-Q. Huang, Y.-T. Sun, J.-X. Xiao, J. Yang, Complex coacervation of soybean protein isolate and chitosan, Food Chem. 135 (2012) 534–539, https://doi.org/10.1016/j.foodchem.2012.04.140.
[43] O. Akakuru, B. Isiuku, Chitosan hydrogels and their glutaraldehyde-crosslinked counterparts as potential drug release and tissue engineering systems-synthesis, characterization, swelling kinetics and mechanism, J. Phys. Chem. Biophys. 7 (2017) 1–7, https://doi.org/10.4172/2161-0398.1000256.
[44] L. Shao, X. Chang, Y. Zhang, Y. Huang, Y. Yao, Z. Guo, Graphene oxide cross-linked chitosan nanocomposite membrane, Appl. Surf. Sci. 280 (2013) 989–992, https://doi.org/10.1016/j.apsusc.2013.04.112.
[45] D.C. Marcano, D.V. Kosynkin, J.M. Berlin, A. Sinitskii, Z. Sun, A. Slesarev, et al., Improved synthesis of graphene oxide, ACS Nano 4 (2010) 4806–4814, https://doi.org/10.1021/nn1006368.
[46] C. Zhu, S. Guo, Y. Fang, S. Dong, Reducing sugar: new functional molecules for the green synthesis of graphene nanosheets, ACS Nano 4 (2010) 2429–2437, https://doi.org/10.1021/nn1002387.
[47] N. Hidayah, W.-W. Liu, C.-W. Lai, N. Noriman, C.-S. Khe, U. Hashim, et al., Comparison on graphite, graphene oxide and reduced graphene oxide: synthesis and characterization, in: AIP Conference Proceedings, AIP Publishing, 2017, https://doi.org/10.1063/1.5005764.
[48] T. Soltani, B.-K. Lee, A benign ultrasonic route to reduced graphene oxide from pristine graphite, J. Colloid Interface Sci. 486 (2017) 337–343, https://doi.org/10.1016/j.jcis.2016.09.075.
[49] Y. Rafitasari, H. Suhendar, N. Imani, F. Luciana, H. Radean, I. Santoso, Sintesis graphene oxide dan reduced graphene oxide, Prosiding seminar nasional fisika (e-journal) (2016), https://doi.org/10.21009/0305020218. SNF2016-MPS-95-98.
[50] P. Sahoo, L. Shubhadarshinee, B.R. Jali, P. Mohapatra, A.K. Barick, Synthesis and characterization of graphene oxide and graphene from coal, Mater. Today: Proc. 56 (2022) 2421–2427, https://doi.org/10.1016/j.matpr.2021.08.206.
[51] A.B. Alayande, S. Chae, I.S. Kim, Surface morphology-dependent spontaneous bacterial behaviors on graphene oxide membranes, Separ. Purif. Technol. 226 (2019) 68–74, https://doi.org/10.1016/j.seppur.2019.05.072.
[52] M. Sabzevari, D.E. Cree, L.D. Wilson, Graphene oxide–chitosan composite material for treatment of a model dye effluent, ACS Omega 3 (2018) 13045–13054, https://doi.org/10.1021/acsomega.8b01871.

[53] N.M. El-Shafai, M.M. Abdelfatah, M.E. El-Khouly, I.M. El-Mehasseb, A. El-Shaer, M.S. Ramadan, et al., Magnetite nano-spherical quantum dots decorated graphene oxide nano sheet (GO@ Fe3O4): electrochemical properties and applications for removal heavy metals, pesticide and solar cell, Appl. Surf. Sci. 506 (2020) 144896, https://doi.org/10.1016/j.apsusc.2019.144896.

[54] K.S. Sing, Reporting physisorption data for gas/solid systems with special reference to the determination of surface area and porosity (Recommendations 1984), Pure Appl. Chem. 57 (1985) 603–619, https://doi.org/10.1351/pac198557040603.

[55] Z.A. Alothman, A review: fundamental aspects of silicate mesoporous materials, Materials 5 (2012) 2874–2902, https://doi.org/10.3390/ma5122874.

[56] P. Jia, H. Tan, K. Liu, W. Gao, Removal of methylene blue from aqueous solution by bone char, Appl. Sci. 8 (2018) 1903, https://doi.org/10.3390/app8101903.

[57] V. Bernal, L. Giraldo, J.C. Moreno-Piraján, Physicochemical properties of activated carbon: their effect on the adsorption of pharmaceutical compounds and adsorbate–adsorbent interactions, C Journal of Carbon Research 4 (2018) 62, https://doi.org/10.3390/c4040062.

[58] D. Savova, N. Petrov, M. Yardim, E. Ekinci, T. Budinova, M. Razvigorova, et al., The influence of the texture and surface properties of carbon adsorbents obtained from biomass products on the adsorption of manganese ions from aqueous solution, Carbon 41 (2003) 1897–1903, https://doi.org/10.1016/S0008-6223(03)00179-9.

[59] K. Kosowska, P. Domalik-Pyzik, M. Nocuń, J. Chłopek, Chitosan and graphene oxide/reduced graphene oxide hybrid nanocomposites–Evaluation of physicochemical properties, Mater. Chem. Phys. 216 (2018) 28–36, https://doi.org/10.1016/j.matchemphys.2018.05.076.

[60] B. Li, C.-L. Shan, Q. Zhou, Y. Fang, Y.-L. Wang, F. Xu, et al., Synthesis, characterization, and antibacterial activity of cross-linked chitosan-glutaraldehyde, Mar. Drugs 11 (2013) 1534–1552, https://doi.org/10.3390/md11051534.

[61] H. Shi, W. Li, L. Zhong, C. Xu, Methylene blue adsorption from aqueous solution by magnetic cellulose/graphene oxide composite: equilibrium, kinetics, and thermodynamics, Ind. Eng. Chem. Res. 53 (2014) 1108–1118, https://doi.org/10.1021/ie4027154.

[62] Q. Fang, Y. Shen, B. Chen, Synthesis, decoration and properties of three-dimensional graphene-based macrostructures: a review, Chem. Eng. J. 264 (2015) 753–771, https://doi.org/10.1016/j.cej.2014.12.001.

[63] W. Xu, Y. Li, H. Wang, Q. Du, M. Li, Y. Sun, et al., Study on the adsorption performance of casein/graphene oxide aerogel for methylene blue, ACS Omega 6 (2021) 29243–29253, https://doi.org/10.1021/acsomega.1c04938.

[64] L. Liang, F. Xi, W. Tan, X. Meng, B. Hu, X. Wang, Review of organic and inorganic pollutants removal by biochar and biochar-based composites, Biochar 3 (2021) 255–281, https://doi.org/10.1007/s42773-021-00101-6.

[65] N. Mohammed, N. Grishkewich, H.A. Waeijen, R.M. Berry, K.C. Tam, Continuous flow adsorption of methylene blue by cellulose nanocrystal-alginate hydrogel beads in fixed bed columns, Carbohydr. Polym. 136 (2016), https://doi.org/10.1016/j.carbpol.2015.09.099, 1194-281.

[66] N. Song, X.-L. Wu, S. Zhong, H. Lin, J.-R. Chen, Biocompatible G-Fe3O4/CA nanocomposites for the removal of methylene blue, J. Mol. Liq. 212 (2015) 63–69, https://doi.org/10.1016/j.molliq.2015.08.059.

[67] P. Senthil Kumar, P.S.A. Fernando, R.T. Ahmed, R. Srinath, M. Priyadharshini, A. Vignesh, et al., Effect of temperature on the adsorption of methylene blue dye onto sulfuric acid–treated orange peel, Chem. Eng. Commun. 201 (2014) 1526–1547, https://doi.org/10.1080/00986445.2013.819352.

[68] W. Konicki, M. Aleksandrzak, D. Moszyński, E. Mijowska, Adsorption of anionic azo-dyes from aqueous solutions onto graphene oxide: equilibrium, kinetic and thermodynamic studies, J. Colloid Interface Sci. 496 (2017) 188–200, https://doi.org/10.1016/j.jcis.2017.02.031.

[69] J.M. Jabar, Y.A. Odusote, K.A. Alabi, I.B. Ahmed, Kinetics and mechanisms of Congo-red dye removal from aqueous solution using activated Moringa oleifera seed coat as adsorbent, Appl. Water Sci. 10 (2020) 1–11, https://doi.org/10.1007/s13201-020-01221-3.

[70] P.S. Kumar, S. Ramalingam, C. Senthamarai, M. Niranjanaa, P. Vijayalakshmi, S. Sivanesan, Adsorption of dye from aqueous solution by cashew nut shell: studies on equilibrium isotherm, kinetics and thermodynamics of interactions, Desalination 261 (2010) 52–60, https://doi.org/10.1016/j.cej.2009.09.013.

[71] S. Subramani, N. Thinakaran, Isotherm, kinetic and thermodynamic studies on the adsorption behaviour of textile dyes onto chitosan, Process Saf. Environ. Protect. 106 (2017) 1–10, https://doi.org/10.1016/j.psep.2016.11.024.

[72] I. Othman, M. Abu Haija, P. Kannan, F. Banat, Adsorptive removal of methylene blue from water using high-performance alginate-based beads, Water, Air, Soil Pollut. 231 (2020) 1–16, https://doi.org/10.1007/s11270-020-04751-3.

[73] W.Z. Durrani, A. Nasrullah, A.S. Khan, T.M. Fagieh, E.M. Bakhsh, K. Akhtar, et al., Adsorption efficiency of date palm based activated carbon-alginate membrane for methylene blue, Chemosphere 302 (2022) 134793, https://doi.org/10.1016/j.chemosphere.2022.134793.

[74] M.A. Al-Ghouti, R.S. Al-Absi, Mechanistic understanding of the adsorption and thermodynamic aspects of cationic methylene blue dye onto cellulosic olive stones biomass from wastewater, Sci. Rep. 10 (2020) 15928, https://doi.org/10.1038/s41598-020-72996-3.

[75] D. Pathania, S. Sharma, P. Singh, Removal of methylene blue by adsorption onto activated carbon developed from Ficus carica bast, Arab. J. Chem. 10 (2017) S1445–S1451, https://doi.org/10.1016/j.arabjc.2013.04.021.

[76] N. Rabiei, M.H. Kish, S.H. Amirshahi, M. Radjabian, The kinetic and thermodynamic parameters of dyeing of polypropylene/Clay composite fibers using disperse dye, Dyes Pigments 94 (2012) 386–392, https://doi.org/10.1016/j.dyepig.2012.02.010.

[77] A.G. Shoaib, S. Ragab, A. El Sikaily, M. Yılmaz, A. El Nemr, Thermodynamic, kinetic, and isotherm studies of Direct Blue 86 dye absorption by cellulose hydrogel, Sci. Rep. 13 (2023) 5910, https://doi.org/10.1038/s41598-023-33078-2.

[78] Y. Shi, G. Song, A. Li, J. Wang, H. Wang, Y. Sun, et al., Graphene oxide-chitosan composite aerogel for adsorption of methyl orange and methylene blue: effect of pH in single and binary systems, Colloids Surf. A Physicochem. Eng. Asp. 641 (2022) 128595, https://doi.org/10.1016/j.colsurfa.2022.128595.

[79] E. Daneshvar, A. Vazirzadeh, A. Niazi, M. Kousha, M. Naushad, A. Bhatnagar, Desorption of methylene blue dye from brown macroalga: effects of operating parameters, isotherm study and kinetic modeling, J. Clean. Prod. 152 (2017) 443–453, https://doi.org/10.1016/j.jclepro.2017.03.119.

[80] A.F. Hassan, H. Elhadidy, Production of activated carbons from waste carpets and its application in methylene blue adsorption: kinetic and thermodynamic studies, J. Environ. Chem. Eng. 5 (2017) 955–963, https://doi.org/10.1016/j.jece.2017.01.003.

[81] I.S. Khattab, F. Bandarkar, M.A.A. Fakhree, A. Jouyban, Density, viscosity, and surface tension of water+ ethanol mixtures from 293 to 323K, Kor. J. Chem. Eng. 29 (2012) 812–817, https://doi.org/10.1007/s11814-011-0239-6.

[82] L. Mouni, L. Belkhiri, J.-C. Bollinger, A. Bouzaza, A. Assadi, A. Tirri, et al., Removal of Methylene Blue from aqueous solutions by adsorption on Kaolin: kinetic and equilibrium studies, Appl. Clay Sci. 153 (2018) 38–45, https://doi.org/10.1016/j.clay.2017.11.034.

[83] S. Mohammad, I. Suzylawati, Study of the adsorption/desorption of MB dye solution using bentonite adsorbent coating, J. Water Proc. Eng. 34 (2020) 101155, https://doi.org/10.1016/j.jwpe.2020.101155.

[84] E.J.C. Amieva, J. López-Barroso, A.L. Martínez-Hernández, C. Velasco-Santos, Graphene-based materials functionalization with natural polymeric biomolecules, Recent advances in graphene research 1 (2016) 257–298, https://doi.org/10.5772/64001.

[85] P.-J. Lu, H.-C. Lin, W.-T. Yu, J.-M. Chern, Chemical regeneration of activated carbon used for dye adsorption, J. Taiwan Inst. Chem. Eng. 42 (2011) 305–311, https://doi.org/10.1016/j.jtice.2010.06.001.

[86] C. Qi, L. Zhao, Y. Lin, D. Wu, Graphene oxide/chitosan sponge as a novel filtering material for the removal of dye from water, J. Colloid Interface Sci. 517 (2018) 18–27, https://doi.org/10.1016/j.jcis.2018.01.089.

[87] L. Fan, C. Luo, M. Sun, X. Li, F. Lu, H. Qiu, Preparation of novel magnetic chitosan/graphene oxide composite as effective adsorbents toward methylene blue, Bioresour. Technol. 114 (2012) 703–706, https://doi.org/10.1016/j.biortech.2012.02.067.

[88] H.M. Hassan, M. El-Aassar, M.A. El-Hashemy, M.A. Betiha, M. Alzaid, A.N. Alqhobisi, et al., Sulfanilic acid-functionalized magnetic GO as a robust adsorbent for the efficient adsorption of methylene blue from aqueous solution, J. Mol. Liq. 361 (2022) 119603, https://doi.org/10.1016/j.molliq.2022.119603.

[89] S. Chang, Q. Zhang, Y. Lu, S. Wu, W. Wang, High-efficiency and selective adsorption of organic pollutants by magnetic CoFe2O4/graphene oxide adsorbents: experimental and molecular dynamics simulation study, Separ. Purif. Technol. 238 (2020) 116400, https://doi.org/10.1016/j.seppur.2019.116400.

[90] T. Huang, Y-w Shao, Q. Zhang, Y-f Deng, Z-x Liang, F-z Guo, et al., Chitosan-cross-linked graphene oxide/carboxymethyl cellulose aerogel globules with high structure stability in liquid and extremely high adsorption ability, ACS Sustain. Chem. Eng. 7 (2019) 8775–8788, https://doi.org/10.1021/acssuschemeng.9b00691.